Universität Zürich[UZH]

Department of Geography

Reconstructing the Pre-Caldera Volcanic Landscape and Magmatic Conditions Prior to the Catastrophic Kos Plateau Tuff Eruption (South Aegean Sea, Greece)

ESS 511 Master's Thesis

Author: Céline Mikosch, 11-730-165

Supervised by: Prof. Dr. Olivier Bachmann (olivier.bachmann@erdw.ethz.ch), Prof. Dr. Markus Egli, Dr. Razvan-Gabriel Popa (razvan.popa@erdw.ethz.ch)

Faculty representative: Prof. Dr. Markus Egli

25.04.2025

Master's Thesis

Reconstructing the Pre-Caldera Volcanic Landscape and Magmatic Conditions Prior to the Catastrophic Kos Plateau Tuff Eruption (South Aegean Sea, Greece)

Presented to the Earth System Science (ESS) Group at
the Department of Geography of the University of Zurich

Under the supervision of (in alphabetical order)

Prof. Dr. Olivier Bachmann, ETH Zurich, Institute of Geochemistry and Petrology,
Faculty representative: Prof. Dr. Markus Egli, University of Zurich, Department of Geography,
Dr. Răzvan-Gabriel Popa, ETH Zurich, Institute of Geochemistry and Petrology

---

Submitted by

Céline Mikosch
11-730-165

Zurich, April 24, 2025

Abstract

Volcanic systems, particularly silicic volcanoes, present significant hazards due to their potential for highly explosive eruptions. Such events can be so devastating that they can completely reshape the landscape, while having a great impact on human populations and climate. However, not much is known about how magma reservoirs can evolve to sizes capable of generating massive eruptions, nor which combination of factors controls their development. Understanding the cyclicity of caldera systems, like Kos, is crucial not only for understanding the evolution of such systems, but also for assessing future volcanic hazards.

This study focuses on the Kos-Nisyros volcanic field in the Aegean Sea, Greece, home of one of the largest active magmatic systems in the region. The catastrophic Kos Plateau Tuff (KPT) eruption, which occurred approximately 0.16 Ma, led to a large-scale caldera collapse with a footprint of roughly 15 x 10 km^2, making it a key site for studying the evolution of large silicic systems. By investigating pre-caldera magmatic lithics from KPT deposits and older volcanic structures, we reconstructed the magmatic history and gained insights into the processes that led to the KPT event. By using petrochronological techniques, such as zircon dating and Hf isotope analyses, alongside bulk-rock chemical analyses, we traced the source, evolution and the zircon crystallization timescales of the magmatic system.

The new zircon crystallization and eruption age data from this study reveal three volcanic pulses preceding the KPT, each characterized by evolving magma evolution toward more silicic compositions. The temporal separation of these pulses by pronounced pauses in zircon crystallization highlights the dynamic and episodic nature of magmatic processes within the Kos–Nisyros caldera system. Zircon crystallization occurred early within the Kos system, with the transition between the incubation and maturation phases being clearly represented by the shift in volcanic products from andesites to dacites, accompanied by relatively high eruption frequencies. As the system evolves toward a large, melt-rich cap over a dominantly mush-rich reservoir, eruption frequency decreases significantly. This trend reflects the progressive maturation of the Kos system, transitioning from frequent intermediate eruptions to more episodic rhyolitic activity. This interpretation is supported by bulk-rock data analyses and Hf isotope values, which reveal a depleted mantle signature with limited crustal assimilation. The pre-KPT rhyolites are crystal-poor, indicating efficient crystal-melt separation through fractional crystallization in mush zones. Particularly, once the final fermentation stage was reached, the upper crustal reservoir stabilized long enough to produce highly differentiated rhyolites, ultimately triggering the catastrophic KPT caldera collapse.

Zusammenfassung

Vulkanische Systeme, insbesondere Vulkane mit silikatischer Schmelze, stellen aufgrund ihres Potenzials für hochexplosive Eruptionen erhebliche Gefahren für Menschen und deren Wirtschaft dar. Das Verständnis der Zyklizität von Calderasystemen wie dem auf Kos ist nicht nur für das Verständnis der Entwicklung solcher Systeme, sondern auch für die Einschätzung künftiger vulkanischer Gefahren von entscheidender Bedeutung.

Diese Studie konzentriert sich auf das Kos-Nisyros-Vulkanfeld im Ägäischen Meer, wo sich eines der grössten magmatischen Systeme der Region befindet. Die katastrophale Eruption des Kos-Plateau-Tuffs (KPT), die sich vor etwa 160'000 Jahren ereignete, führte zu einem grossflächigen Caldera-Kollaps und ist ein Schlüsselstandort für die Untersuchung des Verhaltens und der Entwicklung grosser silikatischer Systeme. Durch die Untersuchung magmatischer Gesteinsfragmente aus KPT-Ablagerungen und prä-eruptiver vulkanischer Strukturen zielt diese Masterarbeit darauf ab, die magmatische Geschichte zu rekonstruieren und die Prozesse zu verstehen, die zum KPT-Ereignis führten. Mithilfe petrochronologischer Techniken wie Zirkon-Datierungen und Hf-Isotopen-Analysen sowie chemischer Analysen der Gesteinszusammensetzung konnte die Entwicklung des Magmas und seiner Kristallisationszeiträume nachgezeichnet werden. Die neuen Daten zur Zirkonkristallisations- und zum Eruptionsalter weisen auf drei verschiedene vulkanische Impulse vor dem KPT hin. Diese sind jeweils durch eine sich entwickelnde Magmazusammensetzung gekennzeichnet, die bis zum Ausbruch des KPT hin, zunehmend silikatreicher wird. Diese drei Impulse sind durch erhebliche Lücken in der Zirkonkristallisation voneinander getrennt, was die Komplexität der Entwicklung des Caldera-Zyklus widerspiegelt. Die Zirkonkristallisation begann bereits früh und markiert den Übergang von der Inkubations- zur Reifungsphase, der sich durch eine Verschiebung der Magmazusammensetzung von Andesiten zu Daziten zeigt, begleitet von einer relativ hohen Eruptionshäufigkeit. Mit der weiteren Entwicklung des magmatischen Systems zu einer großen Magmakammer und der Differenzierung zu kristallarmem, rhyolitischem Magma nimmt die Eruptionshäufigkeit deutlich ab (Reifungsphase). Diese Entwicklung führt zu einem Wechsel von häufigen Eruptionen hin zu seltener, aber (grossvolumiger) magmatischer Aktivität. Die Prä-KPT-Rhyolithe sind kristallarm, was auf eine effiziente Kristall-Schmelze-Trennung durch fraktionierte Kristallisation in den "Mush"-Zonen hinweist. Diese Interpretation wird durch unsere Gesteinszusammensetzungsdaten und Hf-Isotopenwerte gestützt, die auf eine verarmte Mantelsignatur mit geringer Krustenassimilation hinweisen. Besonders während der letzten Fermentationsphase vor dem KPT-Ausbruch stabilisierten sich die oberkrustalen Magmareservoire lange genug, um hochdifferenzierte Rhyolithe zu produzieren, die in der Lage waren, einen Caldera Kollaps auzulösen.

Contents

1 Introduction

With global population growth, an increasing number of people are settling near volcanoes, often unaware of the associated risks. At the same time, volcanoes are becoming increasingly important for the local and global economy. Their fertile, nutrient-rich soils support agriculture, while their abundance of minerals and geothermal energy provide valuable resources for communities (Lockwood et al., 2022; Cashman and Sparks, 2013). Despite their benefits, volcanic eruptions pose a serious threat to human life, particularly the explosive eruptions that are responsible for over 95% of all volcano-related deaths (Brown et al., 2017).
Recent advances have significantly improved our understanding of volcanic hazards (Widiwijayanti et al., 2024; Bachmann and Huber, 2016; Cashman and Sparks, 2013) and the ways in which eruptive styles vary with magmatic storage properties (Popa et al., 2021; Bernard and de Maisonneuve, 2020; Fabbro et al., 2020; Denlinger and Hoblitt, 1999). In general, more silicic magmas can be more dangerous due to their higher volatile contents and higher viscosity, but often show both effusive and explosive eruption styles (Popa et al., 2019; Cassidy et al., 2018; Blake, 1984).
On Earth, silicic volcanoes encompass different types, including relatively small systems erupting magmas of andesitic to dacitic compositions, which can build dome fields (Avellán et al., 2024; Connor et al., 2000) for instance, Aegina (Elburg and Smet, 2020) or Methana, Greece (Pe-Piper and Piper, 2013), or stratovolcanoes, such as Mount St. Helens in the United States (Gardner et al., 1995; Smith and Leeman, 1993), Mount Fuji in Japan (Chakraborty and Jones, 2018; Oguchi and Oguchi, 2010) or Mount Merapi in Indonesia (Gertisser et al., 2012). In contrast, silicic volcanoes can be the result of large magmatic systems that build voluminous subvolcanic magma reservoirs and are able to erupt rhyolites, such as the Kos-Nisyros-Yali volcanic complex in Greece (Bachmann et al., 2012) or Aso volcano in Japan (Keller, 2023; Keller et al., 2023, 2021; Takarada and Hoshizumi, 2020) (Fig. 1).

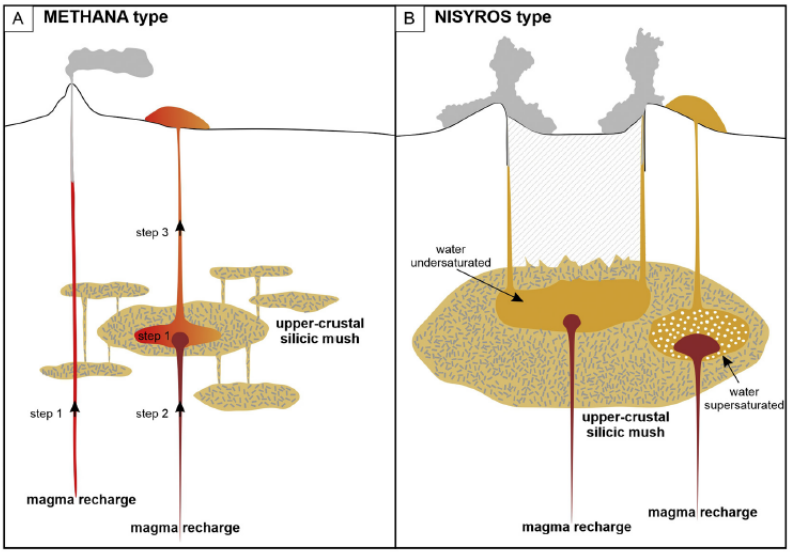

Figure 1: The two general types of silicic arc volcanoes on Earth, according to Bachmann and Huber (2016). (A) Volcanoes producing small to average-sized eruptions with intermediate magma compositions. Their limited magma reservoir volumes typically constrain the evolution of these systems to (rhyo)dacitic compositions. (B) Large, caldera-forming arc volcanoes are capable of erupting tens of km^3 of material in a single event. Their large magmatic mushes can undergo extreme differentiation, resulting in rhyolitic compositions and water supersaturation. Sketch from Popa et al. (2020a).

These large magmatic systems are particularly important because they can trigger caldera collapse events (Lundgren et al., 2020; Anderson et al., 2019; Cashman et al., 2017). Calderas are large volcanic depressions that form during eruptions, as the roof of the magma chamber becomes unstable and collapses, acting like a piston that rapidly extrudes material (Branney and Acocella, 2015; Cashman and Giordano, 2014; Martí et al., 2008; Cole et al., 2005). These eruptions are among the most violent on Earth, capable of destroying entire landscapes through the collapse process and posing significant hazards due to extensive, high-volume pyroclastic flows and falls (Popa et al., 2021; Geshi, 2020; Takarada and Hoshizumi, 2020; McGuire, 2003; Hürlimann et al., 2000; Braitseva et al., 1996).

The outcomes of such eruptions can be exemplified with a few famous caldera collapse examples that occurred in human history, like the Toba caldera in Indonesia which triggered a supervolcanic eruption 74 ka that almost led to the disappearance of the human race (Rose and Chesner, 1990) due to its impact on global climate (Timmreck et al., 2012). Another example is the Santorini caldera collapse event around 1650 BC (Friedrich, 2013; Driessen and MacDonald, 2000; Druitt and Francaviglia, 1992), the consequences of which led to the decline of the Minoan civilization (Driessen and Macdonald, 2020; Bruins et al., 2008; Soles, 2007). A more recent caldera collapse event is the Novarupta eruption in Alaska, which occurred in 1912 and is recognized as the world's largest eruption of the 20^{th} century (Gonnermann and Houghton, 2012; Hildreth and Fierstein, 2012; Hildreth, 1991). Similarly, even in Europe, we can find active volcanoes with a record of caldera collapse events. Those include the Campi Flegrei in Italy (Orsi, 2022; Forni et al., 2018; Orsi et al., 1996) and the Kos-Nisyros-Yali volcanic field in Greece (Bachmann et al., 2019). In addition, an important and recent advancement in understanding these large volcanoes is recognizing that caldera systems follow a cyclicity (de Maisonneuve et al., 2021). This is characterized by developmental stages that contribute to crustal evolution and the nucleation of a magma reservoir, which—through differentiation—reaches a chemically evolved stage enriched in exsolved volatiles (the fermentation stage), and is capable of producing catastrophic eruptions (Locher et al., 2025; de Maisonneuve et al., 2021; Fabbro et al., 2020; Bachmann and Huber, 2016; Bouvet de Maisonneuve et al., 2015). However, at this stage, eruption frequency tends to decrease, as the exsolved volatiles have a dampening effect on the overpressure induced by the recharge magma, though individual eruptions can be more voluminous (Popa et al., 2019; Townsend et al., 2019; Degruyter et al., 2016).

de Maisonneuve et al. (2021) proposed a model (Figure 2) in which, after a magmatic reservoir has incubated, it progresses through three main phases in a caldera cycle. If a sufficient volume of recharge material is introduced into the system, an eruption can still be triggered, and if enough volumes of material are extruded, whether effusively or explosively (Tramontano et al., 2017; Degruyter et al., 2016; Stock et al., 2016), the roof of the magma chamber can destabilize inducing a collapse event. Following a caldera collapse event, the cycle may end and the system die, or it may restart, leading to the buildup of a new cataclysmic event (de Maisonneuve et al., 2021; Keller et al., 2021; Forni et al., 2018).
In the incubation phase, the crust heats up and prepares to build a huge magma reservoir. During maturation, magma differentiates, and the reservoir expands. This is often accompanied by initially frequent volcanic activity, which then decreases over time. Next, in the fermentation phase, volatile exsolution in upper-crustal reservoirs leads to the accumulation of large volumes of eruptible silicic magma, priming the system for caldera collapse. After the collapse, the magma chamber either solidifies and becomes inactive or recovers if sustained deep magmatic recharge occurs, initiating a new cycle. Recognizing and understanding

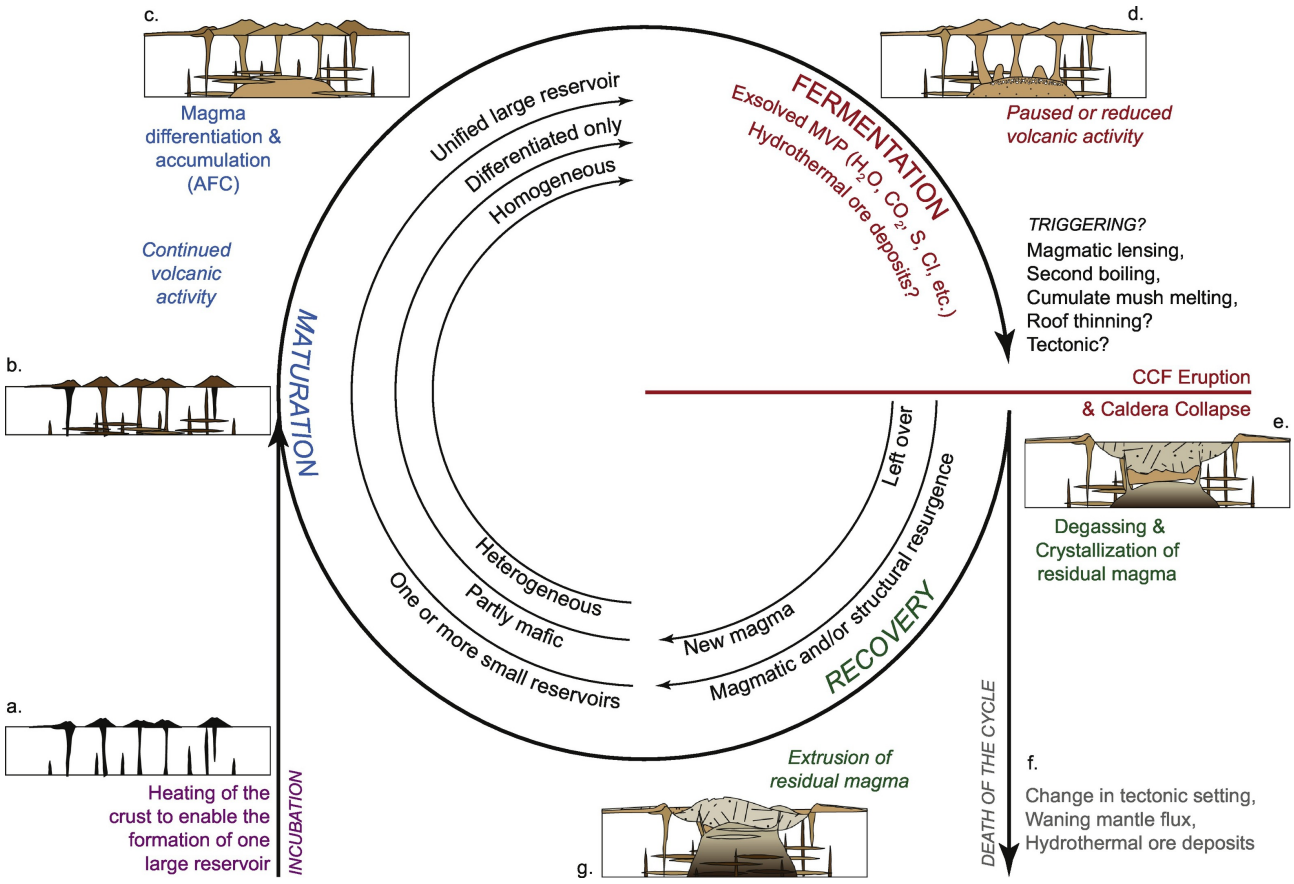

Figure 2: Schematic representation of the caldera cycle in a catastrophic caldera-forming (CCF) volcanic system, from de Maisonneuve et al. (2021). The monocyclic evolution proceeds through (a) an incubation phase, (b–c) maturation marked by assimilation and fractional crystallization (AFC), (d) fermentation with intense magmatic volatile phase (MVP) production, (e) caldera collapse during a CCF eruption, and (f) cessation of activity due to reduced magma input. In contrast, a polycyclic CCF system includes an additional phase (g) of recovery and magmatic recharge following the eruption, enabling the resumption of the cycle.

this cyclicity, especially in systems that are currently dormant but still active, is crucial for accurate risk assessment (de Maisonneuve et al., 2021). Furthermore, a better understanding of the timing and geochemical processes governing caldera cycles can provide valuable insights into the evolution of large magmatic systems and improve predictions of their eruptive behavior. In this context, we examine the active Kos-Nisyros-Yali volcanic system, which experienced multiple explosive and effusive eruptions leading up to the Kos Plateau Tuff (KPT) event.

This study focuses on how the Kos magmatic system developed leading up to the catastrophic KPT caldera collapse event. A key question is identifying the most effective chemical tracers and the main physico-chemical changes that provide insights into the current state of the caldera cycle. To address this, we examine older, pre-KPT eruptions to understand how the magmatic system evolved over time. However, a major challenge in this approach is that the KPT event destroyed much of the older volcanic record during its caldera collapse (de Maisonneuve et al., 2021). Therefore, we rely on studying the volcanic lithics, pieces of broken lavas

and domes, that can be found in the KPT deposits. Those lithics belonged to volcanic structures that were destroyed and can provide valuable insights into the magmatic history. This work includes U-Pb dating to establish crystallization timescales, analyzing chemical indexes for melt evolution, and tracking isotopic evolution of the system which could be related to changes in mantle source fertility. Through this approach, the study aims to provide a deeper understanding of the processes that control caldera cycles on the island of Kos, Greece.

2 Geological Background

The Kos-Nisyros-Yali volcanic field contains the largest magmatic system in the Aegean region (Bachmann et al., 2019), responsible for triggering the most significant Quaternary eruption in this part of the world. This field includes the KPT eruption, which occurred approximately 0.16 Ma (Nomikou et al., 2021; Bachmann et al., 2019; Guillong et al., 2014; Allen, 2001; Smith et al., 1996). The huge scale and impact of the KPT eruption makes the Kos caldera a critical site for studying volcanic hazards and understanding the behavior of large silicic magmatic systems (Bachmann et al., 2012).
Kos, a Greek island in the southeastern part of the Aegean Sea, is located in a geologically important region of the Mediterranean (Fig.3). This area remains one of the most tectonically active zones on Earth (Francalanci and Zellmer, 2019; Vougioukalakis et al., 2019; Nomikou et al., 2018; Bachmann, 2010; Bachmann et al., 2010a; Francalanci et al., 2005; Wortel and Spakman, 2000; Pe-Piper and Piper, 2007; McKenzie, 1972).

According to Papazachos (2019), the broader region of the eastern Mediterranean has some of the highest deformation rates within the entire African-Eurasian plate convergence system. As a result, it is responsible for earthquakes up to magnitude 8.2 (M8.2) and more than 60% of seismicity in Europe. This intense deformation is primarily driven by two major plate movements. The first important factor is the steady northward advance of the African plate towards the Eurasian plate, which exerts significant tectonic forces on the surrounding regions and leading to the subduction of the eastern Mediterranean lithosphere beneath the Aegean Sea (Bachmann et al., 2010a; Fytikas et al., 1976; Papazachos and Comninakis, 1971; Caputo et al., 1970). This subduction process is further complicated by plate retreat, where the sinking lithospheric plate undergoes slab rollback, creating additional tectonic stresses and contributing to the dynamic geological evolution in the region (Bachmann, 2010). Secondly, the westward movement of the Anatolian plate, along the North Anatolian Fault, leads to extensional stresses in the northern Aegean Sea, further shaping the structural framework of the region (Francalanci and Zellmer, 2019; Papazachos, 2019; Pe-Piper and Piper, 2007). The Aegean subduction system comprises three main components, each of which plays a crucial role in the overall tectonic dynamics of the area. The first component is a compressive, non-volcanic arc which includes the southern Peloponnesus Peninsula of Greece and the islands of Crete and Rhodes. The second component is a well-defined volcanic arc, commonly referred to as the South Aegean Volcanic Arc, where extensive magmatic activity has taken place over geological time. This arc, known as the modern Hellenic arc in the Kos-Nisyros region, has been characterized by volcanic activity since the Pliocene, including the eruption of calcareous dacitic domes and rhyolitic domes as well as a tuff ring of the Kefalos series (dated to 3.41 Ma by K-Ar dating) in western Kos (Papazachos, 2019; Allen, 2001; Bellon and Jarrige, 1979). Finally, an extensional back-arc region encompasses the Aegean Sea region north of the volcanic arc, where crustal thinning and rifting processes are actively shaping the landscape (McKenzie, 1972).
The Kos-Nisyros-Yali volcanic field has undergone complex and different eruptive behaviors over the last

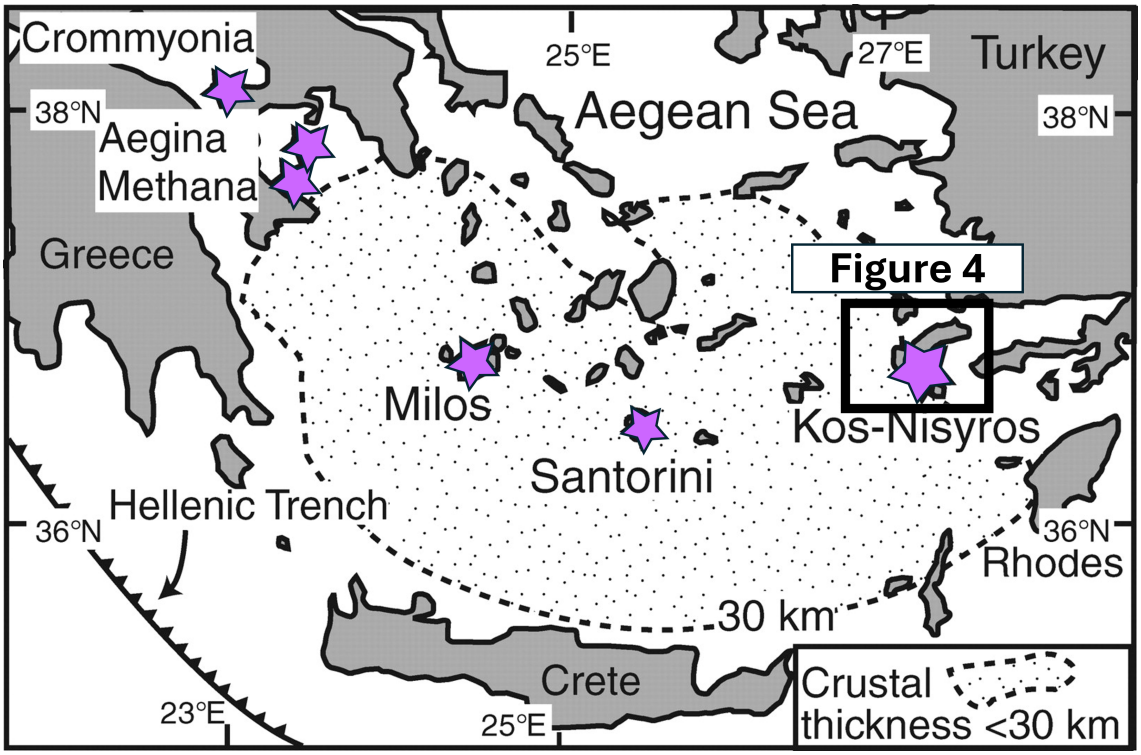

Figure 3: The map shows the major volcanic centers (purple stars) of the South Aegean Volcanic Arc. The Kos-Nisyros volcanic field is located on the easternmost part. The dotted pattern indicates areas where the crust is <30 km thick. The Hellenic Trench is partially shown. Map modified from Bachmann et al. (2007). The black rectangle on the global map highlights the simplified geological map of Kos (Figure 4).

3 Ma, with a spectrum of volcanic activity ranging from effusive eruptions to catastrophic explosive events. Kos is home to the largest volcano in the Aegean Sea and remains a very active magmatic system. This region has seen one of the largest explosive volcanic eruptions in the Mediterranean, the KPT (Bachmann et al., 2012; Allen, 2001; Smith et al., 1996) (Fig.4). It occured at 161 ka and it produced more than 60 km^3 of pyroclastic material, reshaping the surrounding landscape (Bachmann et al., 2019, 2010b, 2007; Allen, 2001; Smith et al., 1996). This eruption left behind a caldera collapse structure that formed a depression about 15 km in diameter between Kos and Nisyros, which is now under water (Bachmann et al., 2019; Allen, 2001). In addition to the 60 km^3 of rhyolitic magma, the KPT also extruded a smaller amount of andesitic material, and incorporated more than 3 km^3 of lithic debris from previously emplaced volcanic rocks and basement (Bachmann et al., 2007). After this major eruptive episode, the magmatic system was reactivated, leading to the development of the Nisyros and Yali volcanoes. These active volcanoes have repeatedly produced rhyolitic eruptions over the last 120 ka, with intermittent explosive activity including minor caldera collapse events (Popa et al., 2020b). The most recent eruptions in this system occurred about 13 ka and marked the last phase of significant volcanic activity (Locher et al., 2025), not to mention the currently active hydrothermal field (Dietrich et al., 2018; Venturi et al., 2018) and the phreatic eruptions that occurred within the Nisyros caldera at the end of the 19^{th} century (Marini et al., 1993).

3 Methodology

Geochemical analyses and sample processing were conducted in the Earth and Planetary Science Department laboratories at ETH Zurich.
The evolution of the magmatic reservoir was investigated using several analytical techniques which are detailed in the subsections below. One of the main tasks involved determining the U-Pb ages of individual zircon crystals, which helped establish eruption ages and crystallization timescales. This also provided insights into the main stages of magma reservoir growth. In addition, geochemical analyses of the bulk-rocks and trace element analyses of zircon crystals helped track the compositional changes of the magmas with time. Another important aspect of this study involved investigating the connection between the magmatic mantle source and the evolution of the volcano. By analyzing hafnium (Hf) isotopes in zircon, valuable information was gained about changes in the source fertility and how these changes related to the long-term development of the volcanic system.

3.1 Sampling and Preparation

The samples were collected during the volcanic field trip in June 2023 on Kos. They originate from volcanic domes, still preserved outside the caldera as well as from broken pieces (lithics) found inside the KPT explosive deposit. The goal of the sampling was to gain a general overview of the area. A total of 24 samples were collected of which only 17 were chosen for further analyses based on hand specimen observations (textures and minerals). Priority was given to samples displaying distinct characteristics and likely to have originated from different eruptions. In addition to the collected samples from this study, two samples were collected from the Kefalos series and from the KPT during the summers of 2022 and 2021, namely OB2022 Kos12 and KPT04-21 (Table 1 and Figure 4).

The sample preparation process involved cutting rocks into smaller fragments and using high-voltage selective fragmentation (SELFRAG) to separate crystals from the matrix. Mineral separation was then carried out using the heavy liquid separation method with Sodium Polytungstate with a density of 2.89 gcm^{-3} to isolate high-density minerals, such as zircon, pyroxene, amphibole, Fe-Ti oxide and apatite from the lighter fraction including quarz, feldspars and volcanic glass.

Zircon were hand-picked under an optical stereomicroscope from the heavy fraction. Between 40 and 70 zircon crystals were picked for each unit and mounted in epoxy resin. The mounts were grinded with aluminum-oxide paper to expose the crystal surfaces and then polished using a diamond suspension down to a grade of 0.25 μm.

Table 1: Overview of the samples collected during this study's volcanological field trip, including corresponding sample names, coordinates, and field notes. The last two samples were not collected during the fieldwork: one was sampled in the summer of 2022 and the other in the summer of 2021, both by Olivier Bachmann, along with their respective sample names, coordinates, and notes.

Sample Name	**Latitude**	**Longitude**	**Notes**
KOS 1*	N36°43'01.1"	E26°57'39.3"	Lava erupted in a sediment basin
KOS 2	N36°43'27.1"	E26°58'12.6"	Hydrated lava with obsidian beads, water interaction
KOS 3	N36°43'24.5"	E26°58'23.1"	Zini Domes, areas with pumice-like, vesiculated glass
KOS 4	N36°43'53.6"	E26°57'19"	Kefalos Series, clastic lithic layer
KOS 5	N36°43'48.1"	E26°57'18.9"	Kefalos Series, pumice
KOS 6.1	N36°46'03.7"	E27°07'14.2"	Lithic in Kos Plateau Tuff
KOS 6.2	N36°46'03.7"	E27°07'14.2"	Lithic in Kos Plateau Tuff
KOS 6.3	N36°46'03.7"	E27°07'14.2"	Lithic in Kos Plateau Tuff
KOS 6.4	N36°46'03.7"	E27°07'14.2"	Lithic in Kos Plateau Tuff
KOS 6.7	N36°46'03.7"	E27°07'14.2"	Lithic in Kos Plateau Tuff
KOS 7.1	N36°46'02.5"	E27°01'13.3"	Pyroclastic flow
KOS 7.4	N36°46'02.5"	E27°01'13.3"	Pyroclastic flow
KOS 8.1	N36°48'28.2"	E27°06'55.5"	Lithic in Kos Plateau Tuff
KOS 8.2	N36°48'28.2"	E27°06'55.5"	Lithic in Kos Plateau Tuff
KOS 9.2	N36°47'28"	E27°01'12"	Lithic
KOS 10	N36°42'14.5"	E26°56'51.7"	Dome
KOS 11	N36°42'14.5"	E26°56'51.7"	Dome
KOS 12	N36°45'38"	E26°59'21"	Large lithic clast, base of Kos Plateau Tuff Kefalos
KPT04-21**	N36°50'12.8"	E27°04'04"	Kos Plateau Tuff pumice

*Only for XRF analyses

**(Bachmann et al., 2012; Bachmann, 2010)

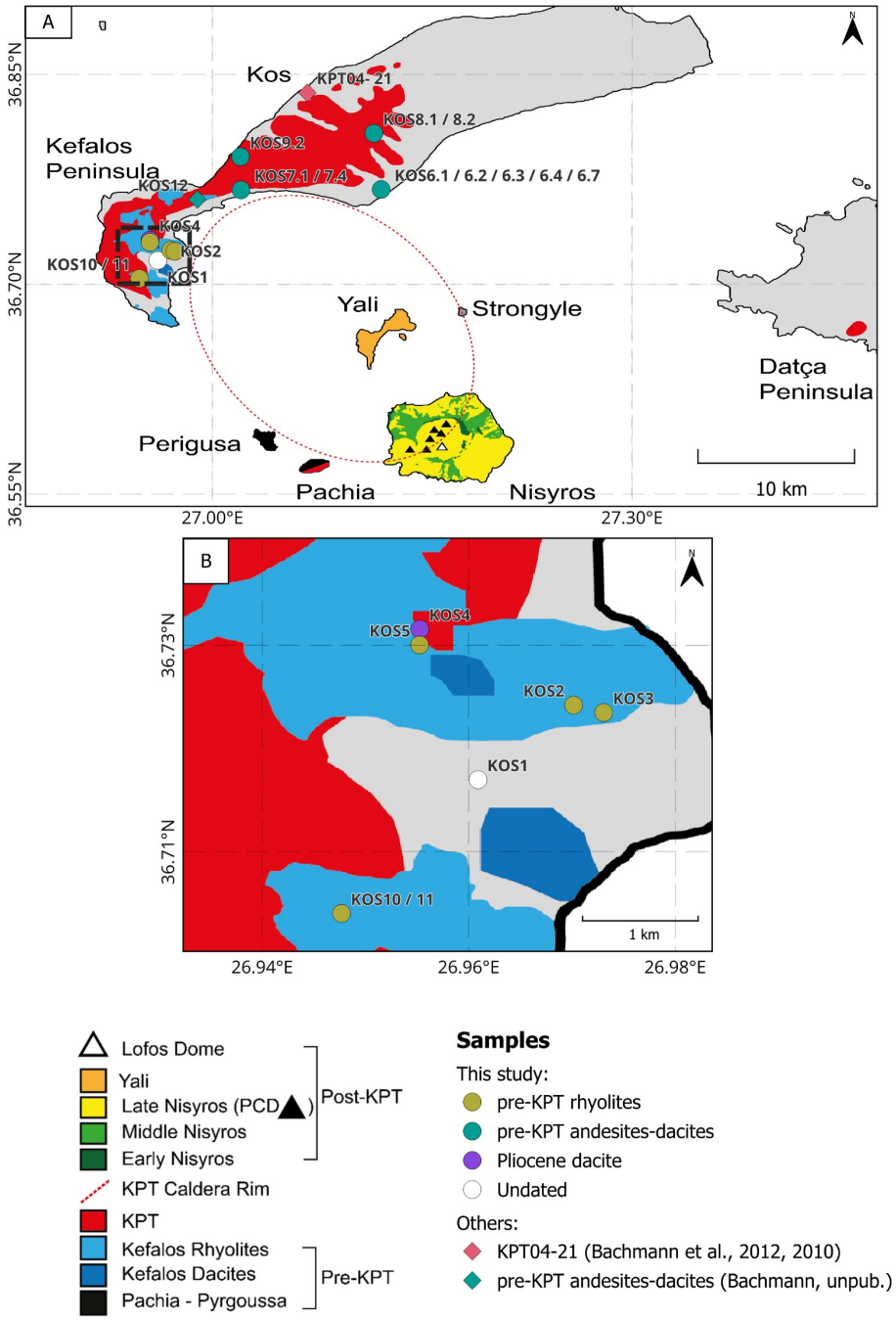

Figure 4: A) The simplified geological map shows the Kos–Nisyros–Yali volcanic field, Greece, illustrating the extent and distribution of volcanic deposits before, during, and after the Kos Plateau Tuff (KPT) eruption. The distribution of volcanic deposits is based on Dietrich and Lagios (2018); Pe-Piper et al. (2005); Allen and McPhie (2001). The red dashed line indicates the rim of the KPT caldera. Colored dots indicate sampling locations used in this study, as listed in Table 1, while diamonds represent samples from Olivier Bachmann (sample KPT04-21 (Bachmann et al., 2012; Bachmann, 2010)). Map modified from Bachmann et al. (2007). B) shows an enlarged view of the Kefalos Peninsula, highlighting a selected area with sampling locations.

3.2 Analytical Methods

3.2.1 LA-ICP-MS: Zircon Dating and Geochemistry

For U-Pb dating of zircon, the Laser Ablation Inductively Coupled Plasma Mass Spectrometry (LA-ICP-MS) method was employed to determine crystallization ages and approximate eruption timings (Guillong et al., 2014; Bachmann et al., 2010a). The zircon isotopic ratios $^{206}Pb/^{238}U$, $^{207}Pb/^{235}U$ and $^{208}Pb/^{232}Th$ were measured using a Resonetics Resolution S155 laser ablation system coupled to a Thermo Element XR sector-field mass spectrometer, operating with a spot diameter of 29 μm, a repetition rate of 5 Hz, and an energy density of 2.5 Jcm^{-2}. The ablation time was set to 30 seconds. GJ-1 (Horstwood et al., 2016; Jackson et al., 2004) served as the primary reference material (RM) (Sliwinski et al., 2022). The accuracy of the method was evaluated by analyzing six zircons with known ages: AUSZ7-1 (Kennedy et al., 2014), AUSZ7-5 (von Quadt et al., 2016), AUSZ8-10 (Lukács et al., 2021), Rak-17 (Webb et al., 2020), 91500 (Horstwood et al., 2016; Wiedenbeck et al., 1995) and Plesovice (Sláma et al., 2008), which served as validation RMs (Sliwinski et al., 2022). NIST 610 glass was used as the RM for the calculation of trace elements concentrations. GJ-1 was measured three times every 20–30 unknowns, with validation RMs analyzed in the middle between the GJ-1 measurement blocks.
The zircon analyses were performed by placing the laser spots primarily near the rims. In some cases, when the zircons were big enough, a second laser spot was placed in the center of the zircon crystals. This allowed us to get a better overview of the crystallization history recorded by the samples (Locher et al., 2025). Additionally, trace elements were also measured together with the isotopic ratios. Data reduction was performed using the Iolite4 software (Paton et al., 2011), which uses the U–Pb geochronology reduction scheme with VisualAge (Petrus and Kamber, 2012), including downhole fractionation correction (Paton et al., 2010). The crystallization age of each zircon phenocryst was determined by applying the common Pb and ^{235}Th–disequilibrium corrections using the DQPB software (Pollard et al., 2023). A constant Th/U fractionation factor D(Th/U) from the melt to the zircon of 0.2 $\pm$ 0.02 (Sakata et al., 2017) was assumed.

For the common Pb correction, the initial $^{207}Pb/^{206}Pb$ ratio was determined using the upper isochron intercept on the Tera-Wasserburg (TW) concordia diagram in IsoplotR (Alagna et al., 2008). However, due to large uncertainties on the measured 7/6 ratios and the isochrone, a fixed initial $^{207}Pb/^{206}Pb$ ratio of 0.8356 calculated with the Stacey Kramers model (Stacey and Kramers, 1975) for an age of 1 Ma was used. Analyses with a high proportion of common Pb, as identified in the TW concordia diagram in IsoplotR, were excluded for the DQPB common Pb and Th disequilibrium correction. This was because the final uncertainties, calculated by Monte Carlo simulation, were either too high or could not be processed by DQPB. In such cases, an incorrect initial $^{207}Pb/^{206}Pb$ ratio could introduce systematic errors. Finally, the eruption ages of the individual samples were estimated by identifying the youngest zircon population, which was determined based on the iterative-Mean Square of the Weighted Deviates (MSWD) after Popa et al. (2020b). The MSWD is a statistical measure used to evaluate how well a set of data points fits a line (such as an isochron) or an average value, taking into account the analytical uncertainties associated with each data point (Guillong et al., 2016). The iterative-MSWD method consists of rejecting outliers or iteratively filtering data to converge on a subset that yields an acceptable MSWD (Popa et al., 2020b).

3.2.2 LA-MC-ICP-MS: Zircon Hafnium-Isotopes

After U-Pb dating, the same zircon crystals were selected for in-situ Hf isotopic analyses. The same spots were used for age and Hf determination. This allowed us to correlate the zircon ages and the isotopic data. The Hf isotopes were determined with a Laser Ablation Multi Collector Inductively Coupled Plasma Mass Spectrometer (LA–MC–ICP–MS), which used Australian Scientific Instruments RESOlution 193 nm ArF excimer laser connected to a Nu Instruments Plasma 2 multicollector inductively coupled plasma mass spectrometer (Woodhead et al., 2004) operating with a spot diameter of 50 μm over 40 seconds, a repetition rate of 5 Hz, and an energy density of 4 Jcm^{-2}. Lolite4 and the Hf isotope data reduction scheme was used to do the data reduction including the correction for interferences of Yb and Lu using the mass bias corrected ratios of ^{176}Yb/^{173}Yb = 0.79502 and ^{176}Lu/^{175}Lu = 0.02656. Additionaly, two different mass bias correction factors were applied. The mass bias correction factor for Hf isotopes was determined based on the natural ratio ^{179}Hf/^{177}Hf = 0.7325 (Chu et al., 2002; Patchett and Tatsumoto, 1981), while the mass bias correction factor for Yb and Lu isotopes was based on the natural ratio ^{173}Yb/^{171}Yb = 1.132685 (Chu et al., 2002). The initial Hf isotopic composition was calculated using the measured ^{176}Hf/^{177}Hf and ^{176}Lu/^{177}Hf ratios, with the crystallization age of the corresponding spot. Moreover, the decay constant of Söderlund et al. (2004) for ^{176}Lu (1.867±0.008 × 10^{-11}) was used. The propagated 2 standard error (S.E.) uncertainty of the initial Hf isotopic composition was determined by the quadratic addition of the 2 S.E. uncertainty within the run and the average 2 standard deviation reproducibility of the initial ^{176}Hf/^{177}Hf ratios of the zircon reference materials. Finally, the ϵHf was calculated using the CHUR (Chondritic Uniform Reservoir) parameters of Bouvier et al. (2008). ϵHf is defined as a normalized expression of the ^{176}Hf/^{177}Hf isotopic ratio in a sample, calculated relative to the CHUR, which represents the average isotopic composition of the Earth's primitive mantle (Waltenberg, 2023).

3.2.3 XRF: Bulk-Rock Chemistry

For bulk-rock chemical analyses, the X-ray Fluorescence (XRF) method was used to measure and quantify elemental concentrations. To prepare the samples for XRF analyses, an aliquot of each sample was first powdered in an agate mill. The powdered samples were then dryed at 110°C for 24 hours. Furthermore, the samples were heated for 2 hours at 950°C to eliminate volatile components. Following this, they were mixed with a Lithium-Tetraborate flux with a ratio 1:5 and subsequently fused at 1080°C to form homogeneous glass beads. This fusing process ensured a homogeneous and representative composition of the bulk-rock sample. Bulk-rock composition measurements were conducted using a Bruker AXS wavelength dispersive X-ray fluorescence Spectrometer S8 TIGER 2nd Series, equipped with a rhodium X-ray tube and 6 diffraction crystals. It is connected to Spectra^{plus}, version 6.61 software. Since the ETH Zurich internal measurement methods are still in the process of being transferred, an application provided by the manufacturer (Bruker AXS) is used. This application was calibrated by the manufacturer using international selected standards and includes a so-called "Master Calibration" (Bruker, 2017). The measurements were conducted within a range of 20-60 kV and 40-170 mA.

4 Results

4.1 Zircon Crystallization and Eruption Ages

A total of 18 samples containing a total of 669 zircon crystals were analyzed using U-Pb geochronology. Zircon crystals were found in all 18 analyzed samples. However, in the pre-KPT rhyolites, particularly in samples Kos 2 (lava), Kos 3 (Zini Dome), Kos 5 (Kefalos Series, pumice), and the two domes Kos 10 and Kos 11, zircon crystals were less abundant, and some were smaller than 100 μm.

Based on the crystallization time span of zircons (Figure 11 in Appendix 6), the samples were subdivided in four main groups. The youngest crystallization period spans from 0.16 to 0.24 Ma and culminated in the KPT eruption. Prior to this, the pre-KPT rhyolites record zircon crystallization between 0.43 to 0.47 Ma while the pre-KPT andesites-dacites, mainly found as lithics within the KPT, show zircon crystallization ages ranging from 0.80 to 1.36 Ma. The oldest sample, found as a lithic fragment in a pre-KPT rhyolite, records a crystallization time span between 2.52 an 3.00 Ma.

After obtaining the crystallization ages, the eruption ages were calculated using two different methods (Figure 5): (1) the youngest zircon population method based on the iterative-MSWD approach after Popa et al. (2020b) and (2) the likelihood-based Bayesian approach using a uniform prior distribution (Keller et al., 2018). The estimated eruption ages for all 18 samples are summarized in Table 2.

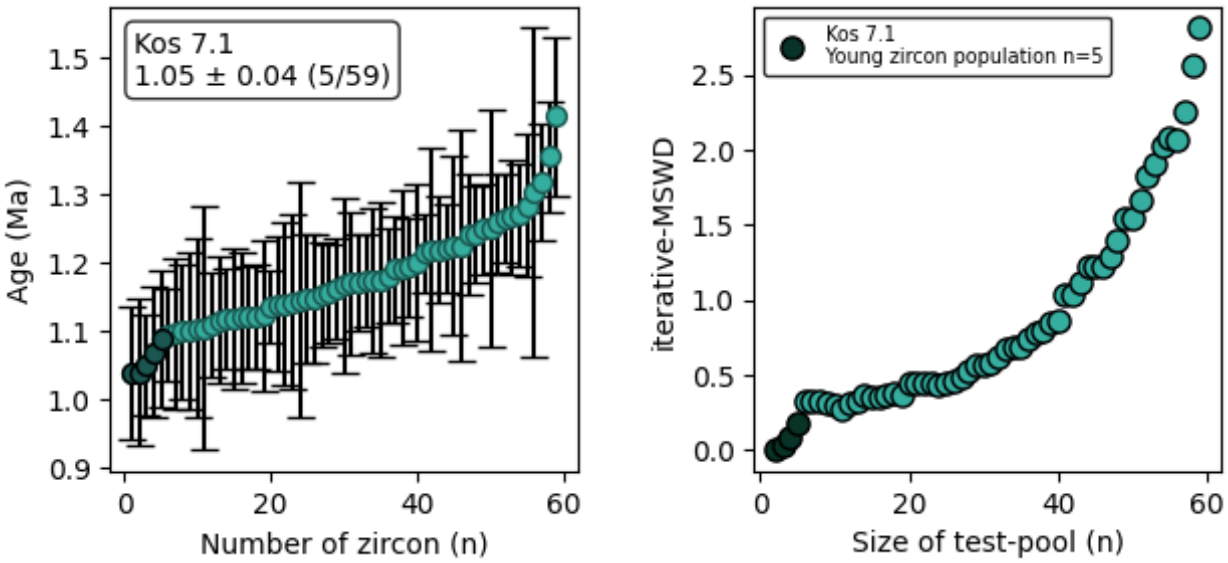

Figure 5: The left figure shows a scatter plot from one specific sample (Kos 7.1). All plots for the remaining samples are shown in Figure 11 in Appendix 6. For sample Kos 7.1 the eruption was estimated at 1.05 Ma. The zircons crystallization timescale for this sample spans from 1.04 to 1.41 Ma. The uncertainty on the individual zircon ages and the eruption age is shown as 2σ. The darker colored dots indicate the number of zircons used for the age estimation of the eruption, in this case, 5 out of 59 zircons.

The right figure illustrates an example of identifying the youngest zircon population using the iterative-MSWD approach. In this example, adding the youngest five zircon ages (n = 5) to the test pool results in relatively small change in the MSWD, especially when compared to the change observed at n=6. The inclusion of the sixth zircon causes a marked jump in the data curve. The zircons with darker colors represent the youngest zircon populations, which is used to estimate the eruption age. In this case, a coherent age population was obtained from the first five youngest crystals before the rate of change in the iterative-MSWD approach makes a jump at n = 6.

According to Popa et al. (2020b), the iterative-MSWD youngest zircon population method involves iteratively calculating the MSWD to identify the youngest coherent zircon population within a dataset (Figure 5b). The MSWD is iteratively calculated by progressively adding the next youngest zircon age to the subset. The iteration begins with the youngest zircon pair (n=2), followed by the stepwise addition of older zircons to the test-pool. At each step, the MSWD is recalculated. Since larger uncertainties in individual ages can obscure important geological processes, such as prolonged crystallization, the youngest zircon population is visually determined by assessing how this parameter changed as more crystals were introduced into the test-pool (Popa et al., 2020b). This process persists until adding another age results in a notable increase—or "jump" in the MSWD value. This jump means that the new age is inconsistent with the previous subset, indicating it belongs to a different age group (Popa et al., 2020b).
The eruption ages were determined by calculating the weighted mean of the youngest zircon population ages weighted by their uncertainty using the equations of IsoplotR (Vermeesch, 2018). For the analyzed samples, the eruption age was based on the youngest age of the population, which was estimated from groups of 2 to 10 crystals. Additionally, the eruption age was estimated using the Bayesian approach (Keller et al., 2018). Due to limited dispersion of the zircon ages a uniform prior distribution was used (Table 2 and Figure 6).

Table 2: Overwiew of estimated eruption ages with the iterative-MSWD (i-MSWD) approach (Popa et al., 2020b) and the Bayesian method with a prior uniform distribution (Keller et al., 2018). The uncertainty is shown as 2σ.

Unit	**i-MSWD (Ma)**	**2σ**	**Bayesian Uniform (Ma)**	**2σ**
KPT (Guillong et al., 2014)	0.158	0.016	0.171	0.011
KPT04-21*	0.164	0.023	0.183	0.022
Kos 2	0.433	0.080	0.466	0.083
Kos 10	0.455	0.066	0.490	0.046
Kos 11	0.468	0.039	0.475	0.043
Kos 5	0.477	0.028	0.478	0.046
Kos 3	0.477	0.035	0.500	0.036
Kos 6.7	0.805	0.046	0.833	0.037
Kos 12	0.843	0.077	0.908	0.040
Kos 6.2	0.862	0.029	0.856	0.032
Kos 7.4	0.951	0.036	0.967	0.032
Kos 8.2	0.999	0.037	1.040	0.034
Kos 6.1	0.976	0.025	0.974	0.030
Kos 6.4	1.033	0.059	1.071	0.032
Kos 7.1	1.049	0.045	1.082	0.031
Kos 6.3	1.089	0.027	1.088	0.031
Kos 8.1	1.163	0.046	1.194	0.040
Kos 9.2	1.361	0.051	1.379	0.055
Kos 4	2.523	0.088	2.593	0.056

*(Bachmann et al., 2012; Bachmann, 2010)

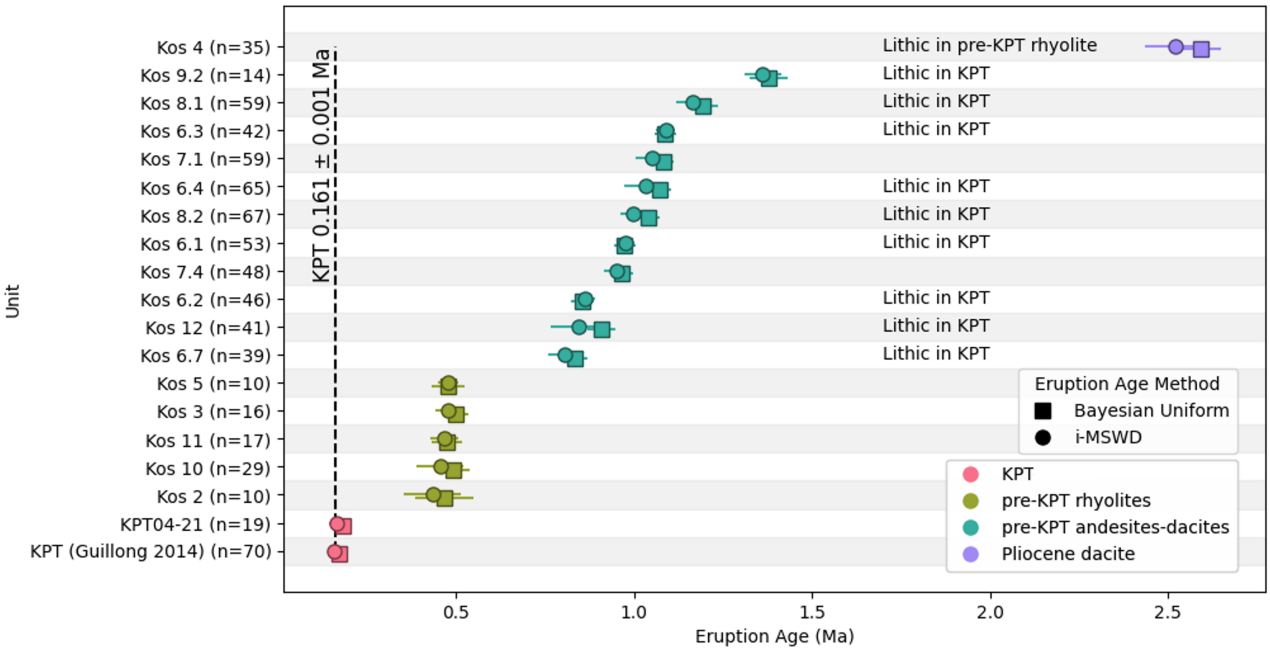

Figure 6: Comparison of eruption ages obtained using two different methods: i-MSWD approach (Popa et al., 2020b) and the Bayesian method with a uniform prior distribution (Keller et al., 2018). The uncertainty is shown as 2σ. Sample names are displayed on the left side of the figure, with the number of individually analyzed zircons indicated in parentheses (n). The dashed line represents the KPT event, dated at 0.161 ± 0.001 Ma (Smith et al., 2000, 1996). Additional KPT data provided by Guillong et al. (2014).

In this specific case, the Bayesian uniform and the youngest zircon population method, based on iterative-MSWD, yield similar eruption ages. However, the eruption ages from the Bayesian method show slightly older ages (Figure 6). Nevertheless, the ages from the Bayesian model and the youngest zircon population are generally within error of each other. The eruption ages of the 19 samples (including the KPT sample from Guillong et al. (2014)) range from 0.16 Ma (KPT) to 2.52 Ma (Pliocene dacite) using the youngest zircon population method and from 0.17 Ma to 2.59 Ma using the Bayesian approach.

4.2 Hf-Isotopes

The Hf-isotopic ratio is expressed as ϵHf. This ratio is age-corrected to account for the radiogenic decay of lutetium (Lu) to Hf over time (Bouvier et al., 2008). For Kos, the ϵHf values with mean uncertainties of range from -1.8 to 9.4 (Figure 7). These values are grouped into four distinct clusters, with no overlap between them. The oldest sample, Pliocene dacite, generally exhibits low ϵHf values clustering between -2 and 3, compared to the other three groups, whose ϵHf values remain mostly above 0. The pre-KPT andesites-dacites, displays a data cloud with values trending from 4 towards 2. The KPT and the pre-KPT rhyolites have a similar ϵHf range, spanning between 3 and 6, while the pre-KPT rhyolites unit shows more scatter with values reaching up to almost 10. By focusing on the weighted mean, a trend of increasing ϵHf from the oldest unit towards the pre-KPT rhyolites can be seen.

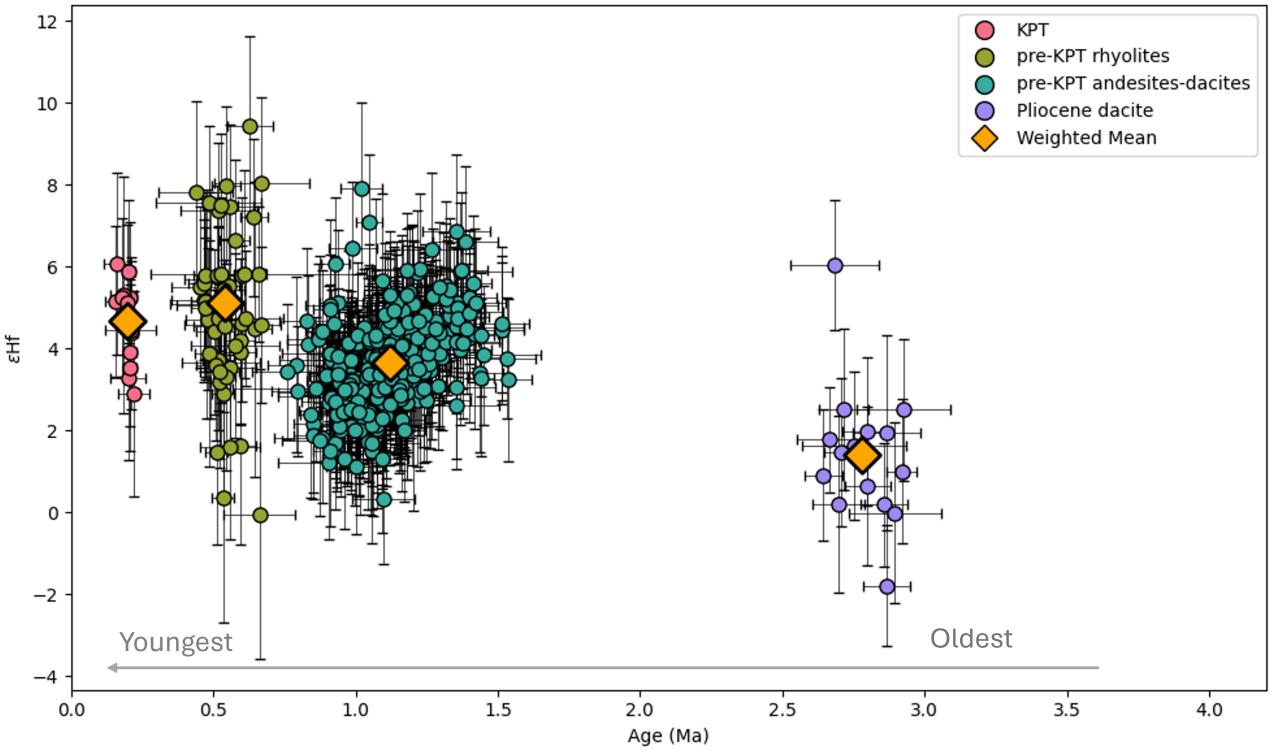

Figure 7: Hf isotopes in zircon plotted over time for 18 Kos samples. The Hf-isotopic variation is expressed as age corrected ϵHf. Uncertainty is shown as 2σ. The color code shows the four different groups, ordered from oldest to youngest. The orange diamonds indicate the ϵHf weighted mean within each group. For Pliocene dacite: ϵHf = 1.41 ± 0.45, pre-KPT andesites-dacites: ϵHf = 3.65 ± 0.10, pre-KPT rhyolites: ϵHf = 5.12 ± 0.28 and KPT: ϵHf = 4.68 ± 0.54.

4.3 Bulk-Rock Chemistry

The bulk-rock composition of all samples, obtained through XRF measurements, is showed in a TAS diagram (Figure 8). Samples from the two oldest groups have a spread between andesitic to dacitic compositions, while the two younger groups are rhyolitic. Specifically, the five analyzed pre-KPT rhyolites are very similar in composition. With younger age the pre-KPT rhyolites and KPT units plot clearly in the rhyolite field.

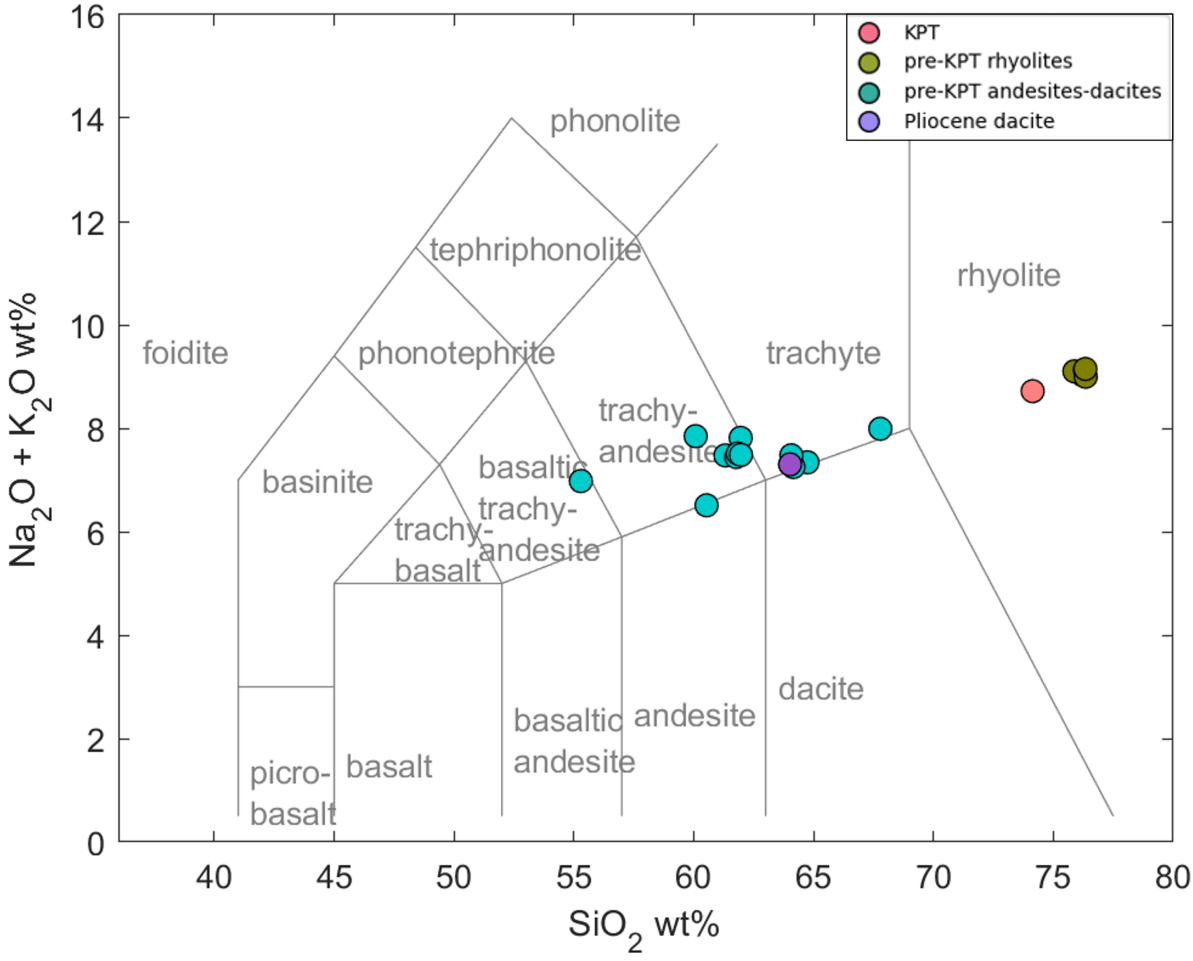

Figure 8: The total alkali vs silica (TAS) diagram (Bas et al., 1986) shows the bulk-rock chemistry of the 18 Kos samples. The silica content clearly rises with the younger ages. The color code corresponds to the four groups, and the data points show a clear chemical evolution from andesitic-dacitic to rhyolitic composition.

A trend is observed in the pre-KPT andesites-dacites, followed by the pre-KPT rhyolites and the post-KPT (Nisyros data from Popa et al. (2020b)) values (Figure 9). The pre-KPT andesites-dacites show a clear increasing trend in SiO2, K2O, and barium (Ba) concentrations. The pre-KPT rhyolites show a concentration of data for SiO2 and K2O around a maximum, with values exceeding 75 wt-% for SiO2 and 4.5 wt-% for K2O. In contrast, the KPT data show a slight decrease, followed by the Nisyros data. This pattern is consistent in the other plot for the trace element Ba. Conversely, the pre-KPT andesites-dacites show a decrease in CaO and Sr, reaching a minimum for the pre-KPT rhyolites. The KPT and post-KPT values show an increasing trend, reaching 4 wt-% for CaO and almost 500 ppm for Sr in the post-KPT samples (Figure 9).

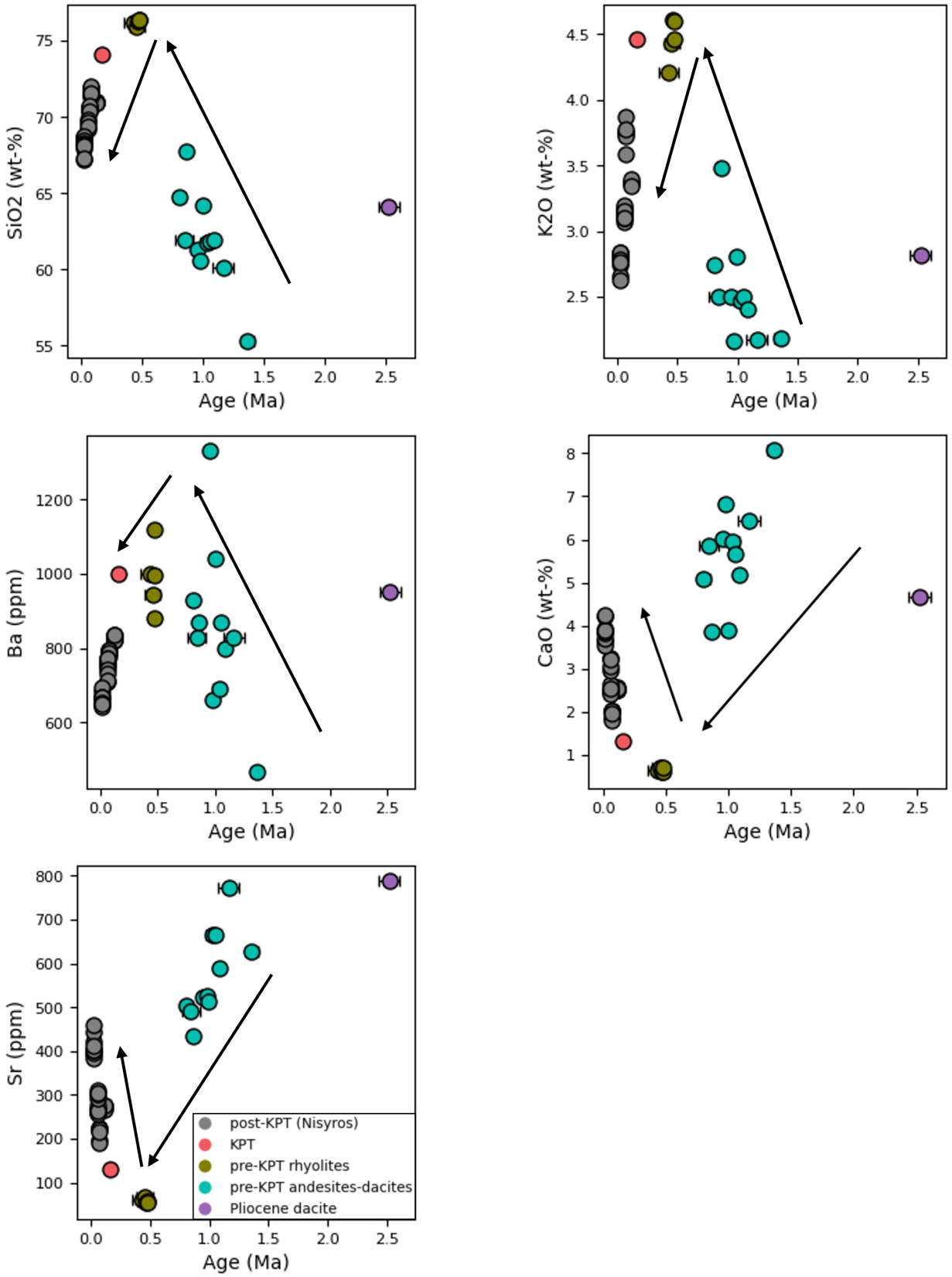

Figure 9: Bulk-rock analyzes from oxides and trace elements plotted against the iterative-MSWD eruption age. The uncertainty is shown as 2σ. Grey data points are from Nisyros from Popa et al. (2020b).

5 Discussion

5.1 Eruption Age Estimates

Even though zircon is not abundant in most rocks, it is very useful for interpreting crustal histories (Cherniak and Watson, 2003). It helps constrain the time span of magmatic processes, such as residence time of magmas in the crust and the intervals between volcanic events, as well as the rate of magma replenishment (Guillong et al., 2014). Zircon can also incorporate trace elements, such as REEs, Y and Hf, which are useful geochemical tracers (Cherniak and Watson, 2003). In addition, they are reliable indicators of magmatic conditions because they are chemically stable during magmatic processes and are commonly found in silicic magmas (Bachmann et al., 2012). Furthermore, U-Pb dating of zircon is a powerful tool to estimate the age of volcanic eruptions (Schmitt, 2011; Bachmann et al., 2007; Bowring and Schmitz, 2003). When zircon crystallizes, it incorporates U and does usually not take common Pb. The U parent isotopes, ^{238}U and ^{235}U, which have two independant decay schemes (Renne et al., 1998), will decay to their radiogenic daughter ^{206}Pb and ^{207}Pb, respectively (Bowring and Schmitz, 2003). As a result, most of the Pb found in zircon is due to radioactive decay (Bowring and Schmitz, 2003). Although zircon typically excludes Pb during crystallization, young zircons have had insufficient time to accumulate significant amounts of radiogenic daughter isotopes. Therefore, even a small amount of common Pb can have a relatively large impact on the isotopic composition and must be carefully accounted for in geochronological analyses. The geochronological clock starts ticking, when zircons in the magma chamber cool below their closure temperature. According to Dodson (1973) the mean closure temperature is around 900°C for zircons of typical size. These magmatic temperatures are very similar to the crystallization temperatures of zircons, which is one reason why the crystallization age of zircon is dated rather than that of other minerals. This allows us to determine the crystallization age of individual zircon crystals and, in turn, estimate the eruption age (Figure 11 in the Appendix 6). Given that rhyolitic magma temperatures were relatively low (Bachmann, 2010), zircon likely crystallized near its closure temperature, meaning the U–Pb ages effectively record the timing of crystallization. Furthermore, assuming that zircon crystallization in the magma chamber continues until the time of eruption (Locher et al., 2025; Bachmann et al., 2007), the age of the youngest zircon population, selected using the iterative-MSWD method according to Popa et al. (2020b), shown in Figure 5 and described in section 4, can serve as a good approximation of the eruption age. On the contrary, older crystals record a prolonged period of growth within the magma reservoir.

The pre-KPT andesites-dacites samples were collected east of the Kefalos Peninsula and are mostly clasts within the KPT (Figure 4; Table 1). In contrast, all pre-KPT rhyolite samples were taken directly from the Kefalos Peninsula (Figure 4). The observed age variations suggest that zircon crystallization occurred over an extended period before the KPT event. These results provide key insights into the timing and duration of zircon formation within the magmatic system. By grouping the zircon crystallization ages based on corresponding eruption ages, the evolution of the magmatic system can be traced. The oldest sample corresponds to a dacitic composition, followed by the gradual evolution of magma toward a more silicic composition. This trend culminates in a silica-rich rhyolitic magma immediately prior to the KPT eruption. Each group of zircon ages is associated with a distinct chemical system, reflecting the compositional changes within the magmatic system over time.

5.2 Pre-KPT Magmatic Activity of Kos in the Context of a Caldera Cycle

The record of zircon crystallization age distribution from the 18 samples shows that Kos experienced three distinct phases of zircon crystallization prior to the catastrophic caldera collapse KPT eruption (Figure 10). These phases are temporally isolated, with no overlap between them, and zircons from later phases do not appear to sample older crystallization events. The crystallization timescale from our oldest sample, the Pliocene dacite, spans a period of approximately 0.5 Ma. As only one of the lithic sample corresponds to this eruption age, this specific crystallization period is represented by only 35 zircon crystallization ages (Figure 11). Nevertheless, this period aligns well with the inferred eruption age of around 2.5 Ma, which is consistent with observations that volcanic activity began on the island of Pachia before 3 Ma and later shifted northeast to the Kefalos Peninsula on Kos, with dacitic magmatism occurring around 2.95 Ma (de Maisonneuve et al., 2021; Pe-Piper and Moulton, 2008).

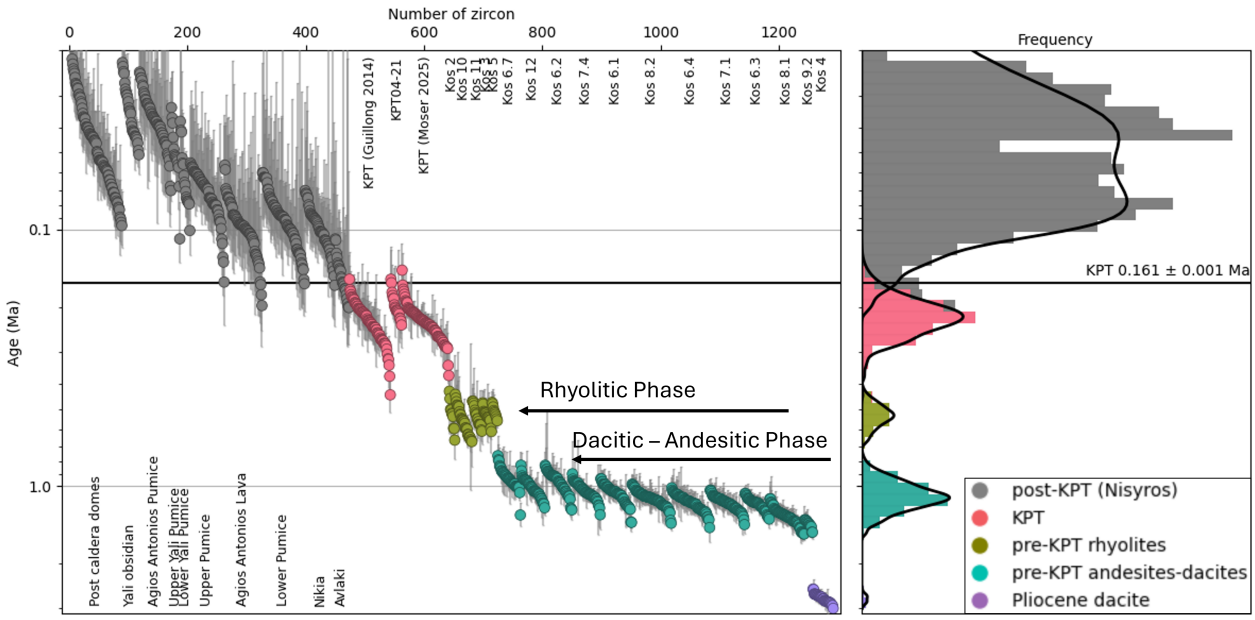

Figure 10: Overview of all zircon crystallization and eruption ages, shown with 2σ uncertainty. The histogram displays the frequency distribution of zircon crystallization ages. Colors reprensent the four sample groups analyzed in this study. KPT data provided by Guillong et al. (2014) and Moser et al. (2025) (manuscript in preparation) were merged with the dataset to provide a more comprehensive overview of crystallization and eruption ages. Grey data points indicate zircon crystallization ages from Nisyros, primarily from (Popa et al., 2020b). Data for the Agios Antonius Pumice and the Agios Antonius Lava units are from Winsemius (unpublished). All datasets were integrated into the study to achieve the most complete possible view of the caldera cycle, from incubation to recovery. Based on the estimated eruption ages, the samples were divided into four groups: Pliocene dacite: 2.52 Ma, pre-KPT andesites-dacites: 1.36 to 0.80 Ma, pre-KPT rhyolites: 0.47 to 0.43 Ma and KPT: 0.16 Ma. The y-axis is shown on a logarithmic scale to better illustrate the range of data.

There is a large eruption age gap (approximately 1.2 Ma) between the Pliocene dacite and the pre-KPT andesites-dacites. One possible explanation for this pause could be an earlier catastrophic event, such as a caldera collapse, which may have emptied the magma reservoir by evacuating most of the silicic material and volatiles (de Maisonneuve et al., 2021), thereby interrupting zircon growth. Subsequently, the system would

have had to rebuild itself inhibiting zircon crystallization during this early recovery phase. To date, there is no clear evidence that another catastrophic caldera collapse event occurred prior to the KPT eruption (de Maisonneuve et al., 2021). This lack of evidence is further supported by the fact that the eruption ages are very well constrained (Popa et al., 2019; Guillong et al., 2014), leaving little room for an earlier catastrophic event to have occurred undetected. Given that the Kos–Nisyros Volcanic Complex has been extensively studied for over forty years, the absence of such evidence in both petrological and geochemical records further diminishes the likelihood of such an event (Dietrich and Popa, 2018; Braschi et al., 2014, 2012; Francalanci et al., 2007; Bachmann et al., 2007; Pe-Piper et al., 2005; Di Paola, 1974). The observed gap can also be explained by a sampling bias, due to limited access to these older units and hence, a limited amount of zircon crystallization ages obtained from only one sample (Figure 10, sample Kos 4). Samples were collected across a wide stratigraphic range with an effort to be representative (Figure 4). However, given the assumption of small and isolated magma chambers during the early stages of the magmatic system (incubation stage, Figure 2), the conservation and subsequent sampling as lithics in the KPT deposit is less likely.

The second magmatic pulse is represented by the eruption age time span from 1.36 to 0.80 Ma, indicating a period of multiple eruptions (Figure 10 and Figure 11). This interval shows a clear and continuous trend in both zircon crystallization and eruption ages. Based on the field observations and hand specimens, we infer that the eruptions during this time span were predominantly effusive, as evidenced by the presence of lithics in the form of lava fragments in the KPT and sampled domes (Figure 6 and Table 1). This suggests a phase of volcanic activity with typical crystal-rich magamas of intermediate composition, evolving over time from andesites to dacites. This trend represents the transition from the incubation stage towards the maturation phase of the caldera cycle (de Maisonneuve et al. (2021), Figure 2). Given that the majority of the sampled lithics represent this magmatic phase and exhibit progressively younger eruption ages, it can be assumed that the eruption frequency was high during this period. However, this assumption cannot be confirmed with certainty, as it is not possible to date every eruption that occurred. The KPT eruption likely destroyed much of the pre-KPT landscape, leaving only limited geological evidence. Our observations are based on a total of 18 available samples, which capture only a fraction of the potentially broader eruptive record. Additionally, it is assumed that the zircons originated from the same magma system—specifically, small upper crustal reservoirs that were likely present during this stage of the caldera cycle (de Maisonneuve et al., 2021). Additionally, it is noteworthy that zircons from the different phases do not predate the previous eruption ages, there are no older zircons found in younger groups. Most of them are antecrysts, and do not show very long tails towards old ages, as expected. This pattern is consistent throughout the entire dataset. Further, there are little to no xenocrysts in the analyzed samples. In contrast, Bachmann et al. (2010a) dated samples from the Kefalos units, Zini and Agios Mammas rhyolitic domes and 3 samples of the Kefalos Series pyroclasts, and found that several zircons were much older than the eruption ages and imply that xenocrysts are in the erupted magma. However, little or no xenocrysts is a sign for limited local crustal assimilation, which is consistent with Bachmann (2010). This interpretation is also supported by geochemical and isotopic signatures in the zircon record, which show a limited amount of assimilation of crustal wall rocks in the area (Bachmann et al., 2007). Furthermore, Bachmann et al. (2012) suggest that the old Paleozoic-Mesozoic basement or Miocene plutons were likely not the primary source of the local dacites and rhyolites. This interpretation is supported by new zircon Hf isotope data, along with existing whole-rock Sr, O, He, Hf, and Nd isotope ratios, which indicate a significant mantle-derived component (Bachmann et al., 2012). The silicic magmas

are interpreted to have evolved through crystal fractionation and minor crustal assimilation (AFC) from intermediate, mantle-influenced parent magmas. The fractional crystallization is the dominant differentiation mechanism in the KPT, espacially in the whole Kos-Nisyros Volcanic Complex (Bachmann et al., 2007).

A third pulse exhibits a much shorter eruption age time span from 0.48 to 0.43 Ma (Figure 11). The eruption ages of the samples representing this pulse are spread very narrowly and fall within each other uncertainties. In contrast to the second magmatic pulse, the third pulse does not follow a continuous trend in eruption ages. Instead, it is preceded by a temporal gap between 0.80 and 0.48 Ma, suggesting a period of volcanic quiescence. This gap is accompanied by a notable shift in magma composition, from older andesite-dacite magmas to more evolved, rhyolitic compositions (Figure 8, rhyolitic field). This shift is not observed within the third pulse itself, but rather marks the transition from the second into the third magmatic pulse. Based on these observations, the sampled lithics either originate from the same eruption, making them very similar in age and chemistry, or they reflect a homogeneous and active magmatic system during that time. The gap between the zircon crystallization of the dacitic-andesitic incubation/maturation phase and the rhyolitic phase spans approximately 0.2 Ma. A potential explanation for the observed gap in zircon crystallization could be sampling bias, where the here studied dataset does not completely resolve the whole crystallization history of the system. However, given the fact, that we potentially sampled five times the same volcanic deposit, it seems unlikely that another big eruption between these two phases would have been missed, although it cannot be entirely excluded.
The younger pre-KPT rhyolitic phase (Figure 10) could represent the potential fermentation stage of the magmatic system (Figure 2). This interpretation is supported by the geochemical homogeneity and closely spaced eruption ages of the sampled rhyolites. If these samples indeed represent a single eruption, it would imply the development of a large, magma reservoir that remained active but un-erupted for a prolonged period, suggesting a phase of internal growth and storage rather than frequent eruptions (de Maisonneuve et al., 2021). The pre-KPT rhyolites do not show many zircon antecrysts extending into the incubation/maturation stage. A possible explanation may be, that during this stage the zircon crystallization was interrupted, suggesting that the magma production rate was maybe too low for zircon growth, and restarted prior to the eruption of rhyolites (Figure 11). According to Bachmann et al. (2012) the Kefalos rhyolites are crystal-poor, with only 2-5 vol% of crystals. Based on Escribano et al. (2022); Bachmann and Bergantz (2004) large magma chamber is needed to generate crystal-poor rhyolites by melt extraction. Therefore, the idea of lower magma production seems unlikely. The crystallization of zircons may have been more continuous than observed, but the antecrysts are not very visible in this study due to the small data set. Based on in-situ observations, the crystals in general were small, and zircons in particular. In these crystal-poor rocks, few zircon crystals that are spaced far apart from each other were found. Further, the pre-KPT rhyolitic magma was relatively cold (Bachmann et al., 2012). According to Escribano et al. (2022) and Bachmann et al. (2012) rhyolitic magmas, especially in their storage conditions prior to eruption or within shallow crustal reservoirs, can be considered relatively cold. Many zircons grew shortly before eruption in these cold, evolved magmas, in which zircons are very stable under such conditions. Moreover, during the incubation stages, the magma chambers may have been relatively small and highly crystalline, effectively becoming dynamically dead. In such a state, these chambers would not have produced many zircons, and most of the existing zircons would have been too stable to be recycled into the rhyolitic magmas. Furthermore, when an eruption occurs, only a specific portion of the magma chamber is tapped, meaning older zircons, though potentially present in the system, were not erupted and therefore remain unrepresented in the samples. As a result, it would not have

been easy to recycle these zircons into the rhyolitic magmas. Recycling zircons from the incubation phase would be challenging due to the highly crystalline nature of the chambers, which limits their potential to contribute antecrysts to the rhyolitic system. Therefore, few zircons from the incubation/maturation stage are expected to be present in the rhyolites.
Additionally, studies from other volcanic systems like Aegina and Methana (Müller, 2023) show that magmatic centers can shift over time. If something similar happened in the Kos-Nisyros volcanic system, the older, crystal-rich magma bodies may have been left behind or disconnected from the younger rhyolitic system. This means that older zircons stored in those earlier magma pockets wouldn't have been mixed into the magmas that eventually erupted—making it less likely to find recycled antecrysts in the current dataset.

For the gap observed between the KPT and the pre-KPT crystal-poor rhyolites the same underlying reasoning discussed previously is proposed. It is assumed that the reservoir(s) of the crystal-poor rhyolites was/were growing, and that the dated zircon population is dominated by the younger phase, formed during the fermentation stage. According to de Maisonneuve et al. (2021), the pre-KPT rhyolites were cold, wet, oxidized and differentiated at the end of the maturation phase/beginning of the fermentation phase (Figure 2), perfect conditions for the pre-KPT rhyolites to produce many zircons. Bachmann et al. (2010a) observed that the zircon populations in these rhyolites often display rims that are significantly younger than their cores. As a result, the ages tend to reflect the younger rim ages, emphasizing the influence of the rims on the overall age distribution.

The data show, a significantly shorter eruption time span for the pre-KPT rhyolites, ranging from 0.48 to 0.43 Ma, compared to the andesites-dacites, which span from 1.36 to 0.80 Ma. This shorter time span suggests that, while the rhyolites may have been less frequent, they could have formed in a more concentrated eruptive event. However, it is important to note that the frequency plot does not directly reflect eruption rates, but rather the distribution of zircon crystallization ages within the dataset. In general, highly evolved, crystal-poor silicic magmas, are volatile-rich and tend to be more prone to eruptions than their crystal-rich counterparts, which are more likely to form plutonic bodies (Parmigiani et al., 2016). Thus, while the data show a smaller frequency peak for the pre-KPT rhyolites, the short eruption time span may still indicate a volcanic activity during that period.
Bachmann (2010) proposed that the parental magma prior to the KPT was a more chemically evolved crystal mush than a fully-solidified granite as propsed by Keller (1969) and that the H_2O-rich crystalline mush was staying above its solidus (670-750°C) before it got reheated and remelted. But as the pre-KPT rhyolites are very crystal poor, they can not originate from a rejuvenated mush like the KPT. According to Parmigiani et al. (2016) the magmatic volatile phase (MVP) plays a key role in highly-evolved, crystal-poor ryholitic systems, where it rises buoyantly in zoned magma reservoirs. In their model the MVP move through a mush (cap-system) that is already formed. The MVP is formed directly by crystallization in the mush, or it is introduced from below by repeated magma recharge. Parmigiani et al. (2016) suggest that the upward MVP is more efficient in regions with high crystallinity, because it leads to the accumulation of MVP bubbles in shallower, less crystalline parts of the magma chamber. In the crystal-poor cap, the MVP is able to form bubble suspension, where the relative velocity of bubbles in relation to the melt is mainly controlled by buoyancy-driven rise. This means the low-density MVP bubbles move upwards through the more viscous melt, with their ascent influenced by interactions with the melt and other bubbles, as well as the reduced buoyancy in the suspension (Parmigiani et al., 2016). Hence, the buildup of low-density MVP bubbles in

crystal-poor magmas can significantly influence their eruptive behavior. The accumulation of bubbles in crystal-poor rhyolitic caps increases their potential energy, promoting eruptions over crustal intrusions. This process helps maintain pressure during eruptions, enabling the near-complete evacuation of magma pockets. As a result, very large volcanic units can form (Parmigiani et al., 2016). de Maisonneuve et al. (2021) suggest that the magmatic system evolves from one or more magma reservoirs that grow, potentially merge, and become increasingly differentiated and volatile-rich. This includes phases with exsolved volatiles and the formation of a crystal mush. Petrologically, it trends from dacite to rhyolite, with evidence of progressive differentiation, shallow storage, decreasing temperatures, and rising volatiles. Volcanic activity is marked by widespread intermediate to silicic eruptions, with initially high but gradually declining eruption frequency.

The pre-KPT rhyolite phase in this study represents the fermentation stage of the magmatic system (Figure 2). Prior to a catastrophic caldera collapse event, the frequency of eruptions appears to decrease, likely allowing the magma reservoir to grow and evolve internally (de Maisonneuve et al., 2021). Although our dataset remains limited, since it is not possible to sample all eruptions predating the KPT eruption, it remains plausible that the eruptive frequency decreased during this fermentation phase. This is supported by field observations from Allen (2001), which identified primarily dacitic domes on the Kefalos Peninsula, and by Dufek and Bergantz (2007), who reported that the majority ($> 80\%$) of lithic fragments within the KPT consist of andesitic clasts. Based on the data of this study and observations, most lithics are indeed andesitic to dacitic in composition, suggesting that rhyolites were not volumetrically dominant during this phase. Consequently, the peak frequency of rhyolites is lower than that of the andesitic–dacitic lithics.
This interpretation is consistent with increasing degrees of magma differentiation, low-pressure storage, decreasing storage temperatures, and rising volatile contents—features that characterize the fermentation phase and align with the evolutionary path described in (de Maisonneuve et al., 2021). These trends likely reflect the development of a single or multiple reservoirs, growing in size (and possibly merging), with a short-lived exsolved magmatic volatile phase and the formation of a crystal mush system. These factors lead to a shift toward conditions that favor large-volume rhyolitic eruptions following a period of maturation and reduced eruptive activity (de Maisonneuve et al., 2021). While those pauses in zircon crystallization observed in the data set (Figure 10) represent a new observation, it should be interpreted with caution. Nonetheless, considering the caldera cycle framework, it is not entirely surprising. We suggest that during the incubation and maturation stages, the chambers were small, and scattered around the area, without much physical contact between them. Hence, the recycling of zircon antecrysts was limited. Further, only during the end of the maturation / beginning of the fermantation stage, as the magmatic system was growing, the smaller isolated magma chambers have merged to build a large integrated magma chamber which ended up producing the KPT.
The youngest frequency peak shows the zircon crystallization ages from Nisyros after the catastrophic caldera event. The gap between the KPT and post-KPT is due to the fact that the silicic material and volatiles in the magma chamber have been largely evacuated during the caldera collapse event. After the KPT event, the frequency of zircon crystallization peak rises again, showing a system that is in the recovery stage (Figure 2), erupting more mafic magmas (Locher et al., 2025). The histogram (Nisyros) exhibits a noticeable dip in the central region, where the frequency of occurrences temporarily decreases before increasing again. This dip corresponds to the two post-Kos Plateau Tuff explosive caldera forming eruptions (Lower Pumice: 0.063 Ma and Upper Pumice: 0.584 Ma) as suggested by Popa et al. (2020b). However, these caldera-forming events are not classified as catastrophic caldera collapses, primarily because their volumes are at least one order of

magnitude smaller than that of the KPT (de Maisonneuve et al., 2021).

Other volcanic systems, e.g. Aegina (Müller, 2023) and Methana, show a shift in the magma reservoirs, which could also be a possibility for the Kos-Nisyros-Yali complex. The spatial evolution of the Kos–Nisyros-Yali volcanic complex show a initial volcanic activity on Pachia around 3 Ma. After it moved to the northeast to the Kefalos Peninsula on Kos (2.95 Ma), ultimately culminating in the catastrophic KPT eruption (de Maisonneuve et al., 2021; Allen, 2001). Following the caldera collapse, volcanic activity migrated southeastward and is currently centered around Nisyros and Yali. Hence, a shift in the magma chambers could disturb the development of large magma chambers and may reflect the incubation/maturation stage. The magma chambers may not coalesce yet but instead form an unconnected magmatic system.

5.3 Mantle Source Evolution

The bulk-rock analyses show a clear temporal trend from andesitic to dacitic to rhyolitic compositions (Figure 8). This chemical evolution is supported by the data (Figure 9) that show trends of increasing SiO_2, K_2O, and Ba along with the decreasing trends of CaO and Sr observed in the pre-KPT magmas from this study. These trends show the evolution of Kos magmas towards a more evolved magma composition. Our data show a silica content approximately around 74.1 and 76.4 wt-% for the rhyolites and 55 to 67.8 wt-% for the andesitics-dacitics. The trend of decreasing CaO and Sr can be explained by the fact that more mafic minerals and plagioclase, both of which incorporate Ca and Sr crystallize and are removed from the melt, thereby depleting the residual liquid in CaO and Sr. The concurrent increase in SiO_2 reflects progressive fractional crystallization, where less-silicic minerals are removed and the melt becomes enriched in silica. Similarly, an increase in K_2O, as Na- and Ca-rich plagioclase crystallizes before K-feldspar during the differentiation process is expected. The behavior of Ba during differentiation is more complex. If plagioclase crystallizes early, Ba remains in the melt because plagioclase does not readily incorporate it. However, the subsequent crystallization of K-feldspar can remove Ba from the melt. This trend is reflected in the observations and is also illustrated in the maturation phase of the caldera cycle (Figure 2), which captures the evolution from mafic to more evolved magmas over time, consistent with the lead-up to the KPT eruption.
In contrast, the study by Locher et al. (2025), which focuses on post-KPT volcanic activity on Nisyros, shows inverse trends. There, CaO and Sr increase, while SiO_2 and Ba decrease (Figure 9). These opposing trends indicate a shift in magmatic processes following the caldera collapse. These observations may suggest that the Nisyros system is still in a recovery phase and is unlikely to produce an imminent catastrophic caldera collapse comparable to the KPT. Additionally, the geochemical differences support the idea that the older domes on Kos are more evolved than the younger domes on Nisyros (Locher et al., 2025).

As shown by Patchett and Tatsumoto (1981), Hf isotopes in zircon provide valuable data on the evolution of mantle reservoirs and the development of mantle heterogeneity. Hence, they offer a significant record of the evolution of fractionated, unfractionated, and crustal contaminated mantle reservoirs over time (Vervoort, 2014; Kinny and Maas, 2003). Positive ϵHf values is due to melt extraction from a depleted source, while negative ϵHf values imply that the magma either came from a more fertile, enriched magma source or was altered by crustal material during its journey upward through the crust.
Bulk-rock compositions and new zircon Hf isotopic data from the Kos samples further reinforce this interpretation. All three types of silicic magmas, Pliocene dacites, pre-KPT andesites-dacites, and pre-KPT rhyolites, follow a common differentiation trend. The Hf isotope analyses on zircons from this study yield a

weighted mean ϵHf of 1.41 for the oldest group, rising to 5.12 for the pre-KPT rhyolites. The KPT rhyolites show a mean ϵHf of 4.68, closely aligning with previously published values by Bachmann et al. (2012) (+5). The Pliocene dacite displays lower ϵHf values, closer to 0, with a weighted mean of 1.41. Further, the zircon of the pre-KPT andesites-dacites indicate a more depleted mantle source, which show a weighted mean from 3.65. The value rises with the pre-KPT rhyolites with an even more depleted mantle reaching a weighted mean value from 5.12.

According to Francalanci and Zellmer (2019), there is a noteworthy east–west variation in isotopic ratios, particularly in Sr and Nd isotopes, which exhibit opposing trends across the South Aegean Volcanic Arc. Sr isotope values are relatively high in the western volcanic centers (e.g. Methana, Aegina), and the range of values is considerably broader compared to those in the eastern islands (Kos, Nisyros, Yali), where both the values and their variability are lower. In contrast, Nd isotopes display the opposite pattern, with more lower values observed in the west and a bit higher values in the east. This inverse relationship is indicative of varying degrees of crustal assimilation and mantle source characteristics across the arc (Francalanci and Zellmer, 2019). The western part of the arc, (e.g Poros, Methana), shows stronger evidence for crustal assimilation in the evolution of rhyolitic magmas (Francalanci and Zellmer, 2019). A comparison of the ϵHf values from Aegina and Methana (Müller, 2023) shows that Methana exhibits low values (-10), wheras Aegina scatters between -5 and 5. However, both show characteristics of a fertile mantle, even though they also exhibit behavior indicative of a depleted mantle (Müller, 2023).

In contrast, the eastern part of the arc (Kos, Nisyros, Yali) reflects a more depleted mantle source with less crustal influence (Francalanci and Zellmer, 2019; Bachmann, 2010). These differences across the arc indicate that, from west to east, less sediment from the subducting plate is being added to the mantle wedge.

Through Nd, Sr, and Pb isotopes it has been shown that the subducted sediment input progressively diminishes eastward along the arc (Francalanci and Zellmer, 2019), which is further influenced by the thicker continental crust in the western part of the South Aegean Arc and the 8 km thick sediment layer on the subducting plate (Papazachos et al., 1995; Woelki et al., 2018). In comparison with these isotopic data, the measurements of Hf values from Kos remain above 0 and follow a clear trend consistent with a depleted mantle. The data from this study are consistent with the data from Francalanci and Zellmer (2019) and confirm that the crustal assimilation for the magmas before the KPT must have been very limited.

6 Conclusions

The new zircon crystallization and eruption age data reveal three distinct volcanic pulses prior to the catastrophic KPT eruption, each associated with evolving magma compositions that become increasingly silicic toward the KPT event. These pulses are separated by significant zircon crystallization gaps, which are not interpreted as caldera collapse events, but rather as reflecting the complex spatial and temporal evolution of the magma reservoir of the Kos-Nisyros caldera system. During the early stage of the Kos-Nisyros system, the magma chambers were most likely small and not interconnected, which aligns with other volcanic systems of the South Aegean Volcanic Arc (e.g. Aegina, Methana) where magmatic centers shifted over time and evolved independently. This could explain the temporal gaps between the observed magmatic episodes. There is also a possibility of a sampling bias due to the limited access to pre-KPT units, as they were destroyed during caldera collapse. The pre-KPT andesites-dacites show a continuous differentiation trend with small but frequent eruptions, representing the maturation stage of the caldera cycle. On the contrary, the

pre-KPT rhyolite samples have almost identical bulk-rock chemistry and do not show continuous eruption ages as they overlap within analytical uncertainties, hence suggesting they originate from the same eruption or eruptive episode. This further implies that eruption frequency decreased while eruptive volume increased, indicating that the system had entered the "growth" stage, marking the transition from the maturation to the fermentation stage of the caldera cycle. The system reaches its limit as it culminates in the catastrophic caldera-forming eruption of the KPT, which destroyed the pre-KPT landscape. The pre-KPT rhyolites are crystal-poor, suggesting efficient crystal–melt separation through crystal fractionation, likely occurring in mush zones at intermediate crystallinity. This is consistent with the bulk-rock chemistry and supported by the Hf isotope data, showing a depleted mantle signature and limited crustal assimilation, thus making fractional crystallization the dominant process for differentiating the system. This agrees with published Sr and Nd isotopes data that show a more pronounced crustal signature in the west and a transition toward a more depleted mantle source in the eastern part of the Aegean Arc.

While the LA-ICP-MS analyses successfully reflect the thermal and temporal evolution of the magma chamber, incorporating cathodoluminescence imaging could help distinguish between primary igneous zoning and potential secondary overgrowths. This would provide valuable insight into the interior structure of the zircons, allowing for the identification of features such as zoning or resorption, thereby refining the temporal resolution of zircon crystallization events.

Acknowledgements

Many thanks to Olivier Bachmann for giving me the great opportunity to write my Master's thesis in his field of research and the possibility to work in his group under his excellent supervision. I am deeply grateful for his clear and concise answers to my questions, as well as for his insightful explanations that often extended beyond them. The exchanges with him were invaluable and greatly enriched my learning. In particular, he was always available in person to answer my questions, even though I did not schedule an appointment in advance, and he consistently responded promptly to my emails.

In addition, I am very grateful to Răzvan-Gabriel Popa for introducing me to this fascinating topic. Further, for his time, for his well-structured and concise answers to my questions, his helpful comments and suggestions, his careful cross-reading of the text, and for his support with data analysis, including detailed explanations and valuable tips. I have greatly benefited from his knowledge.

Thank you to Prof. Dr. Markus Egli for being my supervisor at the University of Zurich, giving important advice and supporting my thesis at all stages.

Many thanks go to Zoe Moser for her strong help with Python and her detailed proofreadings and comments of the text. I am also very grateful to her for her time and long conversations during this thesis period. Next, I am very thankful to Marcel Guillong for his precious assistance during the laser measurements, for answering all my questions regarding the U/Pb and Hf isotope data analyses, as well as for proofreading and commenting on the method part of the thesis. My thanks also go to Natalie Seibel for performing the XRF bulk-rock measurements on the glass beads and for always being open to questions. A big thank you to Rebecca Zech for introducing me to the use of SELFRAG. Special thanks to Simone Marioni for showing me how to use the digital microscope and helping me photograph my mounts, and for being so spontaneous!

I am deeply grateful to Eric Reusser for his invaluable assistance throughout the course of my thesis. I greatly appreciate his thorough proofreading and insightful comments. Beyond his specific help, I am sincerely grateful to Eric for listening to my concerns and offering his guidance.

The warmest thanks go to all my colleagues and friends from office NO F21 for their constant encouragement and pleasant conversations. Special thanks to Andrea Pascatti for introducing me to QGIS, for his patience, and for his invaluable help in improving my geological map. How many hours did we spend on that? In addition, I would like to thank all my colleagues and friends from the 2023 field trip to Kos for helping me collect all the pumice pieces (Kos 5). Special thanks go to Maira Coray, Raphaela Joseph, Hongyi Fu, and Julian Villamizar Blanco for carrying my large and heavy samples back in their luggage. A big thank you goes to Ning Ma for the helpful discussions about geochemistry and volcanoes.

Furthermore, I thank my friend Marc Grandjean for his strong support and sincerely appreciate the enriching conversations we shared throughout the course of the thesis. A warm thank you goes to my friend, Carla Fusco, who cared for Éléonore, giving me the time I needed to write the thesis. A big thank you goes to my family, who have supported me throughout my journey. Last but not least, my deepest thanks go to my husband, Heiner Mikosch, whose steady support over the years made it possible for me to chase my dream - the volcanoes! I will forever be grateful to him.

References

Alagna, K. E., Petrelli, M., Perugini, D., and Poli, G. (2008). Micro-Analytical Zircon and Monazite U-Pb Isotope Dating by Laser Ablation-Inductively Coupled Plasma-Quadrupole Mass Spectrometry. *Geostandards and Geoanalytical research*, 32(1):103–120. DOI: 10.1111/j.1751-908X.2008.00866.x.

Allen, S. (2001). Reconstruction of a Major Caldera-Forming Eruption From Pyroclastic Deposit Characteristics: Kos Plateau Tuff, Eastern Aegean Sea. *Journal of Volcanology and Geothermal Research*, 105(1-2):141–162. DOI: 10.1016/S0377-0273(00)00222-5.

Allen, S. and McPhie, J. (2001). Syn-Eruptive Chaotic Breccia on Kos, Greece, Associated With an Energetic Pyroclastic Flow. *Bulletin of volcanology*, 63:421–432. DOI: 10.1007/s004450100162.

Anderson, K. R., Johanson, I. A., Patrick, M. R., Gu, M., Segall, P., Poland, M. P., Montgomery-Brown, E. K., and Miklius, A. (2019). Magma Reservoir Failure and the Onset of Caldera Collapse at Kīlauea Volcano in 2018. *Science*, 366(6470):eaaz1822. DOI: 10.1126/science.aaz1822.

Avellán, D.-R., Cardona-Melchor, S., Gómez-Vasconcelos, M. G., Macías, J. L., Layer, P. W., Sosa-Ceballos, G., Ruíz, M.-C., Benowitz, J., Cisneros-Máximo, G., Murcia, H., et al. (2024). The Nieve Volcanic Cluster: A Pliocene-Pleistocene Lava Dome Cluster in the Michoacán-Guanajuato Volcanic Field (México). *Journal of Volcanology and Geothermal Research*, 450:108091. DOI: 10.1016/j.jvolgeores.2024.108091.

Bachmann, O. (2010). The Petrologic Evolution and Pre-Eruptive Conditions of the Rhyolitic Kos Plateau Tuff (Aegean Arc). *Open Geosciences*, 2(3):270–305. DOI: 10.2478/v10085-010-0009-4.

Bachmann, O., Allen, S. R., and Bouvet de Maisonneuve, C. (2019). The Kos–Nisyros–Yali Volcanic Field. *Elements: An International Magazine of Mineralogy, Geochemistry, and Petrology*, 15(3):191–196. DOI: 10.2138/gselements.15.3.191.

Bachmann, O. and Bergantz, G. W. (2004). On the Origin of Crystal-Poor Rhyolites: Extracted From Batholithic Crystal Mushes. *Journal of Petrology*, 45(8):1565–1582. DOI: 10.1093/petrology/egh019.

Bachmann, O., Charlier, B., and Lowenstern, J. (2007). Zircon Crystallization and Recycling in the Magma Chamber of the Rhyolitic Kos Plateau Tuff (Aegean arc). *Geology*, 35(1):73–76. DOI: 10.1130/G23151A.1.

Bachmann, O., Deering, C. D., Ruprecht, J. S., Huber, C., Skopelitis, A., and Schnyder, C. (2012). Evolution of Silicic Magmas in the Kos-Nisyros Volcanic Center, Greece: A Petrological Cycle Associated With Caldera Collapse. *Contributions to Mineralogy and Petrology*, 163:151–166. DOI: 10.1007/s00410-011-0663-y.

Bachmann, O. and Huber, C. (2016). Silicic Magma Reservoirs in the Earth's Crust. *American Mineralogist*, 101(11):2377–2404. DOI: 10.2138/am-2016-5675.

Bachmann, O., Schoene, B., Schnyder, C., and Spikings, R. (2010a). The 40Ar/39Ar and U/Pb Dating of Young Rhyolites in the Kos-Nisyros Volcanic Complex, Eastern Aegean Arc, Greece: Age Discordance Due to Excess 40Ar in Biotite. *Geochemistry, Geophysics, Geosystems*, 11(8). DOI: 10.1029/2010GC003073.

Bachmann, O., Wallace, P. J., and Bourquin, J. (2010b). The Melt Inclusion Record From the Rhyolitic Kos Plateau Tuff (Aegean Arc). *Contributions to Mineralogy and Petrology*, 159:187–202. DOI: 10.1007/s00410-009-0423-4.

Bas, M. L., Maitre, R. L., and on the Systematics of Igneous Rocks, I. S. (1986). A Chemical Classification of Volcanic Rocks Based on the Total Alkali-Silica Diagram. *Journal of petrology*, 27(3):745–750. DOI: 10.1093/petrology/27.3.745.

Bellon, H. and Jarrige, J. J. (1979). L'Activité Magmatique Néogene et Quaternaire Dans l'île de Kos, Greece: Données Radiochronologiques. *C.R. Acad. Sci. Paris*, 288:1359–1362.

Bernard, O. and de Maisonneuve, C. B. (2020). Controls on Eruption Style at Rabaul, Papua New Guinea–Insights From Microlites, Porosity and Permeability Measurements. *Journal of Volcanology and Geothermal Research*, 406:107068. DOI: 10.1016/j.jvolgeores.2020.107068.

Blake, S. (1984). Volatile Oversaturation During the Evolution of Silicic Magma Chambers as an Eruption Trigger. *Journal of Geophysical Research: Solid Earth*, 89(B10):8237–8244. DOI: 10.1029/JB089iB10p08237.

Bouvet de Maisonneuve, C., Costa, F., Patia, H., and Huber, C. (2015). Mafic Magma Replenishment, Unrest and Eruption in a Caldera Setting: Insights From the 2006 Eruption of Rabaul (Papua New Guinea). *Geological Society, London, Special Publications*, 422(1):17–39. DOI: 10.1144/SP422.2.

Bouvier, A., Vervoort, J. D., and Patchett, P. J. (2008). The Lu–Hf and Sm–Nd Isotopic Composition of CHUR: Constraints from Unequilibrated Chondrites and Implications for the Bulk Composition of TerrestrialPplanets. *Earth and Planetary Science Letters*, 273(1-2):48–57. DOI: 10.1016/j.epsl.2008.06.010.

Bowring, S. A. and Schmitz, M. D. (2003). High-Precision U-Pb Zircon Geochronology and the Stratigraphic Record. *Reviews in Mineralogy and Geochemistry*, 53(1):305–326. DOI:10.2113/0530305.

Braitseva, O., Melekestsev, I., Ponomareva, V., and Kirianov, V. Y. (1996). The Caldera-Forming Eruption of Ksudach Volcano About Cal. AD 240: The Greatest Explosive Event of Our Era in Kamchatka, Russia. *Journal of Volcanology and Geothermal Research*, 70(1-2):49–65. DOI: 10.1016/0377-0273(95)00047-X.

Branney, M. and Acocella, V. (2015). Calderas. In *The encyclopedia of volcanoes*, pages 299–315. Elsevier. DOI: 10.1016/B978-0-12-385938-9.00016-X.

Braschi, E., Francalanci, L., Tommasini, S., and Vougioukalakis, G. E. (2014). Unraveling the Hidden Origin and Migration of Plagioclase Phenocrysts by In Situ Sr Isotopes: The Case of Final Dome Activity at Nisyros Volcano, Greece. *Contributions to Mineralogy and Petrology*, 167:1–25. DOI:10.1007/s00410-014-0988-4.

Braschi, E., Francalanci, L., and Vougioukalakis, G. E. (2012). Inverse Differentiation Pathway by Multiple Mafic Magma Refilling in the Last Magmatic Activity of Nisyros Volcano, Greece. *Bulletin of volcanology*, 74:1083–1100. DOI:10.1007/s00445-012-0585-1.

Brown, S. K., Jenkins, S. F., Sparks, R. S. J., Odbert, H., and Auker, M. R. (2017). Volcanic Fatalities Database: Analysis of Volcanic Threat With Distance and Victim Classification. *Journal of Applied Volcanology*, 6:1–20. DOI: 10.1186/s13617-017-0067-4.

Bruins, H. J., MacGillivray, J. A., Synolakis, C. E., Benjamini, C., Keller, J., Kisch, H. J., Klügel, A., and Van Der Plicht, J. (2008). Geoarchaeological Tsunami Deposits at Palaikastro (Crete) and the Late Minoan IA Eruption of Santorini. *Journal of Archaeological Science*, 35(1):191–212. DOI: 10.1016/j.jas.2007.08.017.

Bruker (2017). *S8 TIGER, Operator's Manual Original Instructions, Karlsruhe*.

Caputo, M., Panza, G. F., and Postpischl, D. (1970). Deep Structure of the Mediterranean Basin. *Journal of Geophysical Research*, 75(26):4919–4923. DOI: 10.1029/JB075i026p04919.

Cashman, K. V. and Giordano, G. (2014). Calderas and Magma Reservoirs. *Journal of Volcanology and Geothermal Research*, 288:28–45. DOI: 10.1016/j.jvolgeores.2014.09.007.

Cashman, K. V. and Sparks, R. S. J. (2013). How Volcanoes Work: A 25 Year Perspective. *Bulletin*, 125(5-6):664–690. DOI: 10.1130/B30720.1.

Cashman, K. V., Sparks, R. S. J., and Blundy, J. D. (2017). Vertically Extensive and Unstable Magmatic Systems: A Unified View of Igneous Processes. *Science*, 355(6331):eaag3055. DOI: 10.1126/science.aag3055.

Cassidy, M., Manga, M., Cashman, K., and Bachmann, O. (2018). Controls on Explosive-Effusive Volcanic Eruption Styles. *Nature communications*, 9(1):2839. DOI: s41467-018-05293-3.

Chakraborty, A. and Jones, T. E. (2018). Mount Fuji: The Volcano, the Heritage, and the Mountain. *Natural heritage of Japan: Geological, geomorphological, and ecological aspects*, pages 167–175. DOI: 10.1007/978-3-319-61896-8_16.

Cherniak, D. J. and Watson, E. B. (2003). Diffusion in Zircon. *Reviews in mineralogy and geochemistry*, 53(1):113–143. DOI: 10.2113/0530113.

Chu, N.-C., Taylor, R. N., Chavagnac, V., Nesbitt, R. W., Boella, R. M., Milton, J. A., German, C. R., Bayon, G., and Burton, K. (2002). Hf Isotope Ratio Analysis Using Multi-Collector Inductively Coupled Plasma Mass Spectrometry: An Evaluation of Isobaric Interference Corrections. *Journal of Analytical Atomic Spectrometry*, 17(12):1567–1574. DOI: 10.1039/B206707B.

Cole, J., Milner, D., and Spinks, K. (2005). Calderas and Caldera Structures: A Review. *Earth-Science Reviews*, 69(1-2):1–26. DOI: 10.1016/j.earscirev.2004.06.004.

Connor, C. B., Conway, F. M., and Sigurdsson, H. (2000). Basaltic Volcanic Fields. *Encyclopedia of volcanoes*, 1:331–343. DOI: 10.1016/B978-0-12-385938-9.00023-7.

de Maisonneuve, C. B., Forni, F., and Bachmann, O. (2021). Magma Reservoir Evolution During the Build Up to and Recovery From Caldera-Forming Eruptions–A Generalizable Model? *Earth-Science Reviews*, 218:103684. DOI: 10.1016/j.earscirev.2021.103684.

Degruyter, W., Huber, C., Bachmann, O., Cooper, K. M., and Kent, A. J. (2016). Magma Reservoir Response to Transient Recharge Events: The Case of Santorini Volcano (Greece). *Geology*, 44(1):23–26. DOI: 10.1130/G37333.1.

Denlinger, R. P. and Hoblitt, R. P. (1999). Cyclic Eruptive Behavior of Silicic Volcanoes. *Geology*, 27(5):459–462. DOI: 10.1130/0091-7613(1999)027¡0459:CEBOSV¿2.3.CO;2.

Di Paola, G. (1974). Volcanology and Petrology of Nisyros Island (Dodecanese, Greece). *Bulletin Volcanologique*, 38:944–987. DOI: 10.1007/BF02597100.

Dietrich, V. and Lagios, E. (2018). *Nisyros Volcano : The Kos-Yali-Nisyros Volcanic Field*. Active Volcanoes of the World. Springer, Cham, Switzerland.

Dietrich, V. J., Chiodini, G., and Schwandner, F. M. (2018). The Hydrothermal System and Geothermal Activity. *Nisyros Volcano: The Kos-Yali-Nisyros Volcanic Field*, pages 145–201. DOI: 10.1007/978-3-319-55460-0_5.

Dietrich, V. J. and Popa, R.-G. (2018). Petrology and Geochemistry of Lavas and Pyroclastics. *Nisyros Volcano: The Kos-Yali-Nisyros Volcanic Field*, pages 103–144. DOI: 10.1007/978-3-319-55460-0_4.

Dodson, M. H. (1973). Closure Temperature in Cooling Geochronological and Petrological Systems. *Contributions to Mineralogy and Petrology*, 40(3):259–274. DOI: 10.1007/bf00373790.

Driessen, J. and MacDonald, C. F. (2000). The Eruption of the Santorini Volcano and its Effects on Minoan Crete. *Geological Society, London, Special Publications*, 171(1):81–93. DOI: 10.1144/GSL.SP.2000.171.01.08.

Driessen, J. and Macdonald, C. F. (2020). The Troubled Island: Minoan Crete Before and After the Santorini Eruption.

Druitt, T. and Francaviglia, V. (1992). Caldera Formation on Santorini and the Physiography of the Islands in the Late Bronze Age. *Bulletin of Volcanology*, 54:484–493. DOI: 10.1007/BF00301394.

Dufek, J. and Bergantz, G. W. (2007). Dynamics and Deposits Generated by the Kos Plateau Tuff Eruption: Controls of Basal Particle Loss on Pyroclastic Flow Transport. *Geochemistry, Geophysics, Geosystems*, 8(12). DOI: 10.1029/2007GC001741.

Elburg, M. A. and Smet, I. (2020). Geochemistry of Lavas From Aegina and Poros (Aegean Arc, Greece): Distinguishing Upper Crustal Contamination and Source Contamination in the Saronic Gulf Area. *Lithos*, 358:105416. DOI: 10.1016/j.lithos.2020.105416.

Escribano, F. A., Cornet, J., Camilletti, G. C., Otamendi, J. E., Armas, P., Cristofolini, E. A., and Bachmann, O. (2022). Generation of Crystal-Poor Rhyolites From a Shallow Plutonic Reservoir in the Famatinian Arc (Argentina). *Journal of Volcanology and Geothermal Research*, 431:107644. DOI: 10.1016/j.jvolgeores.2022.107644.

Fabbro, G. N., McKee, C. O., Sindang, M. E., Eggins, S., and de Maisonneuve, C. B. (2020). Variable Mafic Recharge Across a Caldera Cycle at Rabaul, Papua New Guinea. *Journal of Volcanology and Geothermal Research*, 393:106810. DOI: 10.1016/j.jvolgeores.2020.106810.

Forni, F., Degruyter, W., Bachmann, O., De Astis, G., and Mollo, S. (2018). Long-Term Magmatic Evolution Reveals the Beginning of a New Caldera Cycle at Campi Flegrei. *Science advances*, 4(11):eaat9401. DOI: 10.1126/sciadv.aat9401.

Francalanci, L., Varekamp, J., Vougioukalakis, G., Innocenti, F., and Manetti, P. (2007). Is There a Compositional Gap at Nisyros Volcano? A Comment on: Magma Generation at the Easternmost Section of the Hellenic Arc: Hf, Nd, Pb and Sr Isotope Geochemistry of Nisyros and Yali Volcanoes (Greece)[Lithos 83 (2005) 29–46]. *Lithos*, 95(3-4):458–461. DOI: 10.1016/j.lithos.2006.06.016.

Francalanci, L., Vougioukalakis, G., Perini, G., and Manetti, P. (2005). A West-East Traverse Along the Magmatism of the South Aegean Volcanic Arc in the Light of Volcanological, Chemical and Isotope Data. In *Developments in Volcanology*, volume 7, pages 65–111. Elsevier. DOI: 10.1016/S1871-644X(05)80033-6.

Francalanci, L. and Zellmer, G. F. (2019). Magma Genesis at the South Aegean Volcanic Arc. *Elements: An International Magazine of Mineralogy, Geochemistry, and Petrology*, 15(3):165–170. DOI: 10.2138/gselements.15.3.165.

Friedrich, W. L. (2013). The Minoan Eruption of Santorini Around 1613 BC and its Consequences. *Tagungen des Landesmuseums für Vorgeschichte Halle*, 9(2013):37–48.

Fytikas, M., Giuliani, O., Innocenti, F., Marinelli, G. t., and Mazzuoli, R. (1976). Geochronological Data on Recent Magmatism of the Aegean Sea. *Tectonophysics*, 31(1-2):T29–T34. DOI: 10.1016/0040-1951(76)90161-X.

Gardner, J. E., Carey, S., Rutherford, M. J., and Sigurdsson, H. (1995). Petrologic Diversity in Mount St. Helens Dacites During the Last 4,000 Years: Implications for Magma Mixing. *Contributions to Mineralogy and Petrology*, 119:224–238. DOI: 10.1007/BF00307283.

Gertisser, R., Charbonnier, S. J., Keller, J., and Quidelleur, X. (2012). The Geological Evolution of Merapi Volcano, Central Java, Indonesia. *Bulletin of Volcanology*, 74:1213–1233. DOI: 10.1007/s00445-012-0591-3.

Geshi, N. (2020). Volcanological Challenges to Understanding Explosive Large-Scale Eruptions. *Earth, Planets and Space*, 72:1–10. DOI: 10.1186/s40623-020-01222-1.

Gonnermann, H. M. and Houghton, B. (2012). Magma Degassing During the Plinian Eruption of Novarupta, Alaska, 1912. *Geochemistry, Geophysics, Geosystems*, 13(10). DOI: 10.1029/2012GC004273.

Guillong, M., Sliwinski, J. T., Schmitt, A., Forni, F., and Bachmann, O. (2016). U-Th zircon Dating by Laser Ablation Single Collector Inductively Coupled Plasma-Mass Spectrometry (LA-ICP-MS). *Geostandards and Geoanalytical Research*, 40(3):377–387. DOI: 10.1111/j.1751-908X.2016.00396.x.

Guillong, M., von Quadt, A., Sakata, S., Peytcheva, I., and Bachmann, O. (2014). LA-ICP-MS Pb–U Dating of Young Zircons From the Kos–Nisyros Volcanic Centre, SE Aegean Arc. *Journal of Analytical Atomic Spectrometry*, 29(6):963–970. DOI: 10.1039/C4JA00009A.

Hildreth, W. (1991). The Timing of Caldera Collapse at Mount Katmai in Response to Magma Withdrawal Toward Novarupta. *Geophysical Research Letters*, 18(8):1541–1544. DOI: 10.1029/91GL01083.

Hildreth, W. and Fierstein, J. (2012). *The Novarupta-Katmai Eruption of 1912: Largest Eruption of the Twentieth Century: Centennial Perspectives*. US Department of the Interior, US Geological Survey Reston, VA, USA.

Horstwood, M. S., Košler, J., Gehrels, G., Jackson, S. E., McLean, N. M., Paton, C., Pearson, N. J., Sircombe, K., Sylvester, P., Vermeesch, P., et al. (2016). Community-Derived Standards for LA-ICP-MS U-(Th-) Pb Geochronology–Uncertainty Propagation, Age Interpretation and Data Reporting. *Geostandards and Geoanalytical Research*, 40(3):311–332. DOI: 10.1111/j.1751-908X.2016.00379.x.

Hürlimann, M., Martí, J., and Ledesma, A. (2000). Mechanical Relationship Between Catastrophic Volcanic Landslides and Caldera Collapses. *Geophysical research letters*, 27(16):2393–2396. DOI: 10.1029/2000GL011564.

Jackson, S. E., Pearson, N. J., Griffin, W. L., and Belousova, E. A. (2004). The Application of Laser Ablation-Inductively Coupled Plasma-Mass Spectrometry to in Situ U–Pb Zircon Geochronology. *Chemical geology*, 211(1-2):47–69. DOI: 10.1016/j.chemgeo.2004.06.017.

Keller, C. B., Schoene, B., and Samperton, K. M. (2018). A Stochastic Sampling Approach to Zircon Eruption Age Interpretation. *Geochemical Perspectives Letters (Online)*, 8(LLNL-JRNL-738859). DOI: 10.7185/geochemlet.1826.

Keller, F. (2023). *Understanding Long-Term Petrological Cycles in Silicic Calderas of Japan*. PhD thesis, ETH Zurich.

Keller, F., Bachmann, O., Geshi, N., and Miyakawa, A. (2021). The Role of Crystal Accumulation and Cumulate Remobilization in the Formation of Large Zoned Ignimbrites: Insights From the Aso-4 Caldera-Forming Eruption, Kyushu, Japan. *Frontiers in Earth Science*, 8:614267. DOI: 10.3389/feart.2020.614267.

Keller, F., Guillong, M., Geshi, N., Miyakawa, A., and Bachmann, O. (2023). Tracking Caldera Cycles in the Aso Magmatic System–Applications of Magnetite Composition as a Proxy for Differentiation. *Journal of Volcanology and Geothermal Research*, 436:107789. DOI: 10.1016/j.jvolgeores.2023.107789.

Keller, J. (1969). Origin of Rhyolites by Anatectic Melting of Granitic Crustal Rocks: The Example of Rhyolitic Pumice From the Island of Kos (Agean Sea). *Bulletin Volcanologique*, 33:942–959. DOI: 10.1007/BF02596758.

Kennedy, A. K., Wotzlaw, J.-F., Schaltegger, U., Crowley, J. L., and Schmitz, M. (2014). Eocene Zircon Reference Material for Microanalysis of U-Th-Pb Isotopes and Trace Elements. *The Canadian Mineralogist*, 52(3):409–421. DOI: 10.3749/canmin.52.3.409.

Kinny, P. D. and Maas, R. (2003). Lu–Hf and Sm–Nd Isotope Systems in Zircon. *Reviews in mineralogy and geochemistry*, 53(1):327–341. DOI: 10.2113/0530327.

Locher, V., Popa, R.-G., Guillong, M., and Bachmann, O. (2025). Insights Into Caldera Cycles Obtained From the Eruption Ages and Chemistry of the Youngest Products of Nisyros Volcano, South Aegean Arc. *Journal of Volcanology and Geothermal Research*, page 108281. DOI: 10.1016/j.jvolgeores.2025.108281.

Lockwood, J. P., Hazlett, R. W., and de la Cruz-Reyna, S. (2022). *Volcanoes: Global Perspectives*. John Wiley & Sons.

Lukács, R., Guillong, M., Bachmann, O., Fodor, L., and Harangi, S. (2021). Tephrostratigraphy and Magma Evolution Based on Combined Zircon Trace Element and U-Pb Age Data: Fingerprinting Miocene Silicic Pyroclastic Rocks in the Pannonian Basin. *Frontiers in Earth Science*, 9:615768. DOI: 10.3389/feart.2021.615768.

Lundgren, P., Girona, T., Bato, M. G., Realmuto, V. J., Samsonov, S., Cardona, C., Franco, L., Gurrola, E., and Aivazis, M. (2020). The Dynamics of Large Silicic Systems From Satellite Remote Sensing Observations: The Intriguing Case of Domuyo Volcano, Argentina. *Scientific reports*, 10(1):11642. DOI: 10.1038/s41598-020-67982-8.

Marini, L., Principe, C., Chiodini, G., Cioni, R., Fytikas, M., and Marinelli, G. (1993). Hydrothermal Eruptions of Nisyros (Dodecanese, Greece). Past Events and Present Hazard. *Journal of Volcanology and Geothermal Research*, 56(1-2):71–94. DOI: 10.1016/0377-0273(93)90051-R.

Martí, J., Geyer, A., Folch, A., and Gottsmann, J. (2008). A Review on Collapse Caldera Modelling. *Developments in Volcanology*, 10:233–283. DOI: 10.1016/S1871-644X(07)00006-X.

McGuire, W. (2003). Volcano Instability and Lateral Collapse. *Revista*, 1:33–45.

McKenzie, D. (1972). Active Tectonics of the Mediterranean Region. *Geophysical Journal International*, 30(2):109–185. DOI: 10.1111/j.1365-246X.1972.tb02351.x.

Moser, Z., Popa, R.-G., Guillong, M., Halldórsson, S. A., Jónasson, K., Nathwani, C., and Bachmann, O. (2025). *Improving Crystallization and Eruption Ages Estimations Using U-Th and U-Pb Dating of Young Volcanic Zircons*. Manuscript in preparation.

Müller, M. (2023). *Understanding a Volcano From Inception to Death: Case Study of Aegina Volcano, Greece*. Master's Thesis, ETH Zurich.

Nomikou, P., Krassakis, P., Kazana, S., Papanikolaou, D., and Koukouzas, N. (2021). The Volcanic Relief Within the Kos-Nisyros-Tilos Tectonic Graben at the Eastern Edge of the Aegean Volcanic Arc, Greece and Geohazard Implications. *Geosciences*, 11(6):231. DOI: 10.3390/geosciences11060231.

Nomikou, P., Papanikolaou, D., and Dietrich, V. J. (2018). Geodynamics and Volcanism in the Kos-Yali-Nisyros Volcanic Field. *Nisyros volcano: the Kos-Yali-Nisyros volcanic field*, pages 13–55. DOI: 10.1007/978-3-319-55460-0_2.

Oguchi, T. and Oguchi, C. T. (2010). Mt. Fuji: The Beauty of a Symmetric Stratovolcano. *Geomorphological landscapes of the world*, pages 303–309. DOI: 10.1007/978-90-481-3055-9_31.

Orsi, G. (2022). Volcanic and Deformation History of the Campi Flegrei Volcanic Field, Italy. *Campi Flegrei: A Restless Caldera in a Densely Populated Area*, pages 1–53.

Orsi, G., De Vita, S., and Di Vito, M. (1996). The Restless, Resurgent Campi Flegrei Nested Caldera (Italy): Constraints on its Evolution and Configuration. *Journal of Volcanology and Geothermal Research*, 74(3-4):179–214. DOI: 10.1016/S0377-0273(96)00063-7.

Papazachos, B. and Comninakis, P. (1971). Geophysical and Tectonic Features of the Aegean Arc. *Journal of Geophysical Research*, 76(35):8517–8533. DOI: 10.1029/JB076i035p08517.

Papazachos, C., Hatzidimitriou, P., Panagiotopoulos, D., and Tsokas, G. (1995). Tomography of the Crust and Upper Mantle in Southeast Europe. *Journal of Geophysical Research: Solid Earth*, 100(B7):12405–12422. DOI: 10.1029/95JB00669.

Papazachos, C. B. (2019). Deep Structure and Active Tectonics of the South Aegean Volcanic Arc. *Elements: An International Magazine of Mineralogy, Geochemistry, and Petrology*, 15(3):153–158. DOI: 10.2138/gselements.15.3.153.

Parmigiani, A., Faroughi, S., Huber, C., Bachmann, O., and Su, Y. (2016). Bubble Accumulation and its Role in the Evolution of Magma Reservoirs in the Upper Crust. *Nature*, 532(7600):492–495. DOI: 10.1038/nature17401.

Patchett, P. and Tatsumoto, M. (1981). A Routine High-Precision Method for Lu-Hf Isotope Geochemistry and Chronology. *Contributions to Mineralogy and Petrology*, 75:263–267. DOI: 10.1007/BF01166766.

Paton, C., Hellstrom, J., Paul, B., Woodhead, J., and Hergt, J. (2011). Iolite: Freeware for the Visualisation and Processing of Mass Spectrometric Data. *Journal of Analytical Atomic Spectrometry*, 26(12):2508–2518. DOI: 10.1039/C1JA10172B.

Paton, C., Woodhead, J. D., Hellstrom, J. C., Hergt, J. M., Greig, A., and Maas, R. (2010). Improved Laser Ablation U-Pb Zircon Geochronology Through Robust Downhole Fractionation Correction. *Geochemistry, Geophysics, Geosystems*, 11(3). DOI: 10.1029/2009GC002618.

Pe-Piper, G. and Moulton, B. (2008). Magma Evolution in the Pliocene–Pleistocene Succession of Kos, South Aegean Arc (Greece). *Lithos*, 106(1-2):110–124. DOI: 10.1016/j.lithos.2008.07.002.

Pe-Piper, G. and Piper, D. J. (2007). Neogene Backarc Volcanism of the Aegean: New Insights Into the Relationship Between Magmatism and Tectonics. DOI: 10.1130/2007.2418(02).

Pe-Piper, G. and Piper, D. J. (2013). The Effect of Changing Regional Tectonics on an Arc Volcano: Methana, Greece. *Journal of Volcanology and Geothermal Research*, 260:146–163. DOI: 10.1016/j.jvolgeores.2013.05.011.

Pe-Piper, G., Piper, D. J., and Perissoratis, C. (2005). Neotectonics and the Kos Plateau Tuff Eruption of 161 ka, South Aegean Arc. *Journal of Volcanology and Geothermal Research*, 139(3-4):315–338. DOI: 10.1016/j.jvolgeores.2004.08.014.

Petrus, J. A. and Kamber, B. S. (2012). VizualAge: A Novel Approach to Laser Ablation ICP-MS U-Pb Geochronology Data Reduction. *Geostandards and Geoanalytical Research*, 36(3):247–270. DOI: 10.1111/j.1751-908X.2012.00158.x.

Pollard, T., Woodhead, J., Hellstrom, J., Engel, J., Powell, R., and Drysdale, R. (2023). DQPB: Software for Calculating Disequilibrium U–Pb Ages. *Geochronology*, 5(1):181–196. DOI: 10.5194/gchron-5-181-2023.

Popa, R.-G., Bachmann, O., Ellis, B. S., Degruyter, W., Tollan, P., and Kyriakopoulos, K. (2019). A Connection Between Magma Chamber Processes and Eruptive Styles Revealed at Nisyros-Yali Volcano (Greece). *Journal of Volcanology and Geothermal Research*, 387:106666. DOI: 10.1016/j.jvolgeores.2019.106666.

Popa, R.-G., Bachmann, O., and Huber, C. (2021). Explosive or Effusive Style of Volcanic Eruption Determined by Magma Storage Conditions. *Nature Geoscience*, 14(10):781–786. DOI: 10.1038/s41561-021-00827-9.

Popa, R.-G., Dietrich, V. J., and Bachmann, O. (2020a). Effusive-Explosive Transitions of Water-Undersaturated Magmas. The Case Study of Methana Volcano, South Aegean Arc. *Journal of Volcanology and Geothermal Research*, 399:106884. DOI: 10.1016/j.jvolgeores.2020.106884.

Popa, R.-G., Guillong, M., Bachmann, O., Szymanowski, D., and Ellis, B. (2020b). U-Th Zircon Dating Reveals a Correlation Between Eruptive Styles and Repose Periods at the Nisyros-Yali Volcanic Area, Greece. *Chemical Geology*, 555:119830. DOI: 10.1016/j.chemgeo.2020.119830.

Renne, P. R., Karner, D. B., and Ludwig, K. R. (1998). Absolute Ages Aren't Exactly. *Science*, 282(5395):1840–1841. DOI: 10.1126/science.282.5395.1840.

Rose, W. I. and Chesner, C. A. (1990). Worldwide Dispersal of Ash and Gases From Earth's Largest Known Eruption: Toba, Sumatra, 75 ka. *Palaeogeography, Palaeoclimatology, Palaeoecology*, 89(3):269–275. DOI: 10.1016/0031-0182(90)90068-I.

Sakata, S., Hirakawa, S., Iwano, H., Danhara, T., Guillong, M., and Hirata, T. (2017). A New Approach for Constraining the Magnitude of Initial Disequilibrium in Quaternary Zircons by Coupled Uranium and Thorium Decay Series Dating. *Quaternary Geochronology*, 38:1–12. DOI: 10.1016/j.quageo.2016.11.002.

Schmitt, A. K. (2011). Uranium Series Accessory Crystal Dating of Magmatic Processes. *Annual Review of Earth and Planetary Sciences*, 39(1):321–349. DOI: 10.1146/annurev-earth-040610-133330.

Sláma, J., Košler, J., Condon, D. J., Crowley, J. L., Gerdes, A., Hanchar, J. M., Horstwood, M. S., Morris, G. A., Nasdala, L., Norberg, N., et al. (2008). Plešovice Zircon—A New Natural Reference Material for U–Pb and Hf Isotopic Microanalysis. *Chemical geology*, 249(1-2):1–35. DOI: 10.1016/j.chemgeo.2007.11.005.

Sliwinski, J. T., Guillong, M., Horstwood, M. S., and Bachmann, O. (2022). Quantifying Long-Term Reproducibility of Zircon Reference Materials by U-Pb LA-ICP-MS Dating. *Geostandards and Geoanalytical Research*, 46(3):401–409. DOI: 10.1111/ggr.12442.

Smith, D. R. and Leeman, W. P. (1993). The Origin of Mount St. Helens Andesites. *Journal of Volcanology and Geothermal Research*, 55(3-4):271–303. DOI: 10.1016/0377-0273(93)90042-P.

Smith, P., York, D., Chen, Y., and Evensen, N. (1996). Single Crystal 40Ar-39Ar Dating of a Late Quaternary Paroxysm on Kos, Greece: Concordance of Terrestrial and Marine Ages. *Geophysical Research Letters*, 23(21):3047–3050. DOI: 10.1029/96GL02759.

Smith, P. E., Evensen, N. M., and York, D. (2000). Under the Volcano: A New Dimension in Ar-Ar Dating of Volcanic Ash. *Geophysical research letters*, 27(5):585–588. DOI: 10.1029/1999GL008451.

Söderlund, U., Patchett, P. J., Vervoort, J. D., and Isachsen, C. E. (2004). The 176Lu Decay Constant Determined by Lu–Hf and U–Pb Isotope Systematics of Precambrian Mafic Intrusions. *Earth and Planetary Science Letters*, 219(3-4):311–324. DOI: 10.1016/S0012-821X(04)00012-3.

Soles, J. S. (2007). The Impact of the Minoan Eruption of Santorini on Mochlos, a Small Minoan Town on the North Coast of Crete. *Monographs of the Danish Institute at Athens (MoDIA)*, 10:107–116.

Stacey, J. t. and Kramers, J. (1975). Approximation of Terrestrial Lead Isotope Evolution by a Two-Stage Model. *Earth and planetary science letters*, 26(2):207–221. DOI: 10.1016/0012-821X(75)90088-6.

Stock, M. J., Humphreys, M. C., Smith, V. C., Isaia, R., and Pyle, D. M. (2016). Late-Stage Volatile Saturation as a Potential Trigger for Explosive Volcanic Eruptions. *Nature Geoscience*, 9(3):249–254. DOI: 10.1038/ngeo2639.

Takarada, S. and Hoshizumi, H. (2020). Distribution and Eruptive Volume of Aso-4 Pyroclastic Density Current and Tephra Fall Deposits, Japan: A M8 Super-Eruption. *Frontiers in Earth Science*, 8:170. DOI: 10.3389/feart.2020.00170.

Timmreck, C., Graf, H.-F., Zanchettin, D., Hagemann, S., Kleinen, T., and Krüger, K. (2012). Climate Response to the Toba Super-Eruption: Regional Changes. *Quaternary International*, 258:30–44. DOI: 10.1016/j.quaint.2011.10.008.

Townsend, M., Huber, C., Degruyter, W., and Bachmann, O. (2019). Magma Chamber Growth During Intercaldera Periods: Insights From Thermo-Mechanical Modeling With Applications to Laguna Del Maule, Campi Flegrei, Santorini, and Aso. *Geochemistry, Geophysics, Geosystems*, 20(3):1574–1591. DOI: 10.1029/2018GC008103.

Tramontano, S., Gualda, G. A., and Ghiorso, M. S. (2017). Internal Triggering of Volcanic Eruptions: Tracking Overpressure Regimes for Giant Magma Bodies. *Earth and Planetary Science Letters*, 472:142–151. DOI: 10.1016/j.epsl.2017.05.014.

Venturi, S., Tassi, F., Vaselli, O., Vougioukalakis, G. E., Rashed, H., Kanellopoulos, C., Caponi, C., Capecchiacci, F., Cabassi, J., Ricci, A., et al. (2018). Active Hydrothermal Fluids Circulation Triggering Small-Scale Collapse Events: The Case of the 2001–2002 Fissure in the Lakki Plain (Nisyros Island, Aegean Sea, Greece). *Natural Hazards*, 93:601–626. DOI: 10.1007/s11069-018-3318-8.

Vermeesch, P. (2018). IsoplotR: A Free and Open Toolbox for Geochronology. *Geoscience Frontiers*, 9(5):1479–1493. DOI: 10.1016/j.gsf.2018.04.001.

Vervoort, J. (2014). Lu-Hf Dating: The Lu-Hf Isotope System. *Encyclopedia of scientific dating methods*, pages 1–20. DOI:10.1007/978-94-007-6326-5_46-1.

von Quadt, A., Wotzlaw, J.-F., Buret, Y., Large, S. J., Peytcheva, I., and Trinquier, A. (2016). High-Precision Zircon U/Pb Geochronology by ID-TIMS Using New 10 13 Ohm Resistors. *Journal of Analytical Atomic Spectrometry*, 31(3):658–665. DOI: 10.1039/C5JA00457H.

Vougioukalakis, G. E., Satow, C. G., and Druitt, T. H. (2019). Volcanism of the South Aegean Volcanic Arc. *Elements: An International Magazine of Mineralogy, Geochemistry, and Petrology*, 15(3):159–164. DOI:10.2138/gselements.15.3.159.

Waltenberg, K. (2023). Application of the Lu–Hf Isotopic System to Ore Geology, Metallogenesis and Mineral Exploration. In *Isotopes in Economic Geology, Metallogenesis and Exploration*, pages 189–208. Springer.

Webb, P., Wiedenbeck, M., and Glodny, J. (2020). G-Chron 2019–Round 1: An International Proficiency Test for U-Pb Geochronology Laboratories; Report on the 2019 Round of G-Chron based on Palaeozoic Zircon Rak-17 (Distribution: September 2019). DOI: 10.48440/GFZ.B103-2.

Widiwijayanti, C., Thin Zar Win, N., Espinosa-Ortega, T., Costa, F., and Taisne, B. (2024). The Global Volcano Monitoring Infrastructure Database (GVMID). *Frontiers in Earth Science*, 12:1284889. DOI: 10.3389/feart.2024.1284889.

Wiedenbeck, M., Alle, P., Corfu, F., Griffin, W. L., Meier, M., Oberli, F. v., Quadt, A. v., Roddick, J., and Spiegel, W. (1995). Three Natural Zircon Standards for U-Th-Pb, Lu-Hf, Trace Element and REE Analyses. *Geostandards newsletter*, 19(1):1–23. DOI: 10.1111/j.1751-908X.1995.tb00147.x.

Woelki, D., Haase, K. M., Schoenhofen, M. V., Beier, C., Regelous, M., Krumm, S. H., and Günther, T. (2018). Evidence for Melting of Subducting Carbonate-Rich Sediments in the Western Aegean Arc. *Chemical Geology*, 483:463–473. DOI: 10.1016/j.chemgeo.2018.03.014.

Woodhead, J., Hergt, J., Shelley, M., Eggins, S., and Kemp, R. (2004). Zircon Hf-Isotope Analysis With an Excimer Laser, Depth Profiling, Ablation of Complex Geometries, and Concomitant Age Estimation. *Chemical Geology*, 209(1-2):121–135. DOI: 10.1016/j.chemgeo.2004.04.026.

Wortel, M. and Spakman, W. (2000). Subduction and Slab Detachment in the Mediterranean-Carpathian Region. *Science*, 290(5498):1910–1917. DOI: 10.1126/science.290.5498.1910.

List of Figures

List of Tables

Appendix

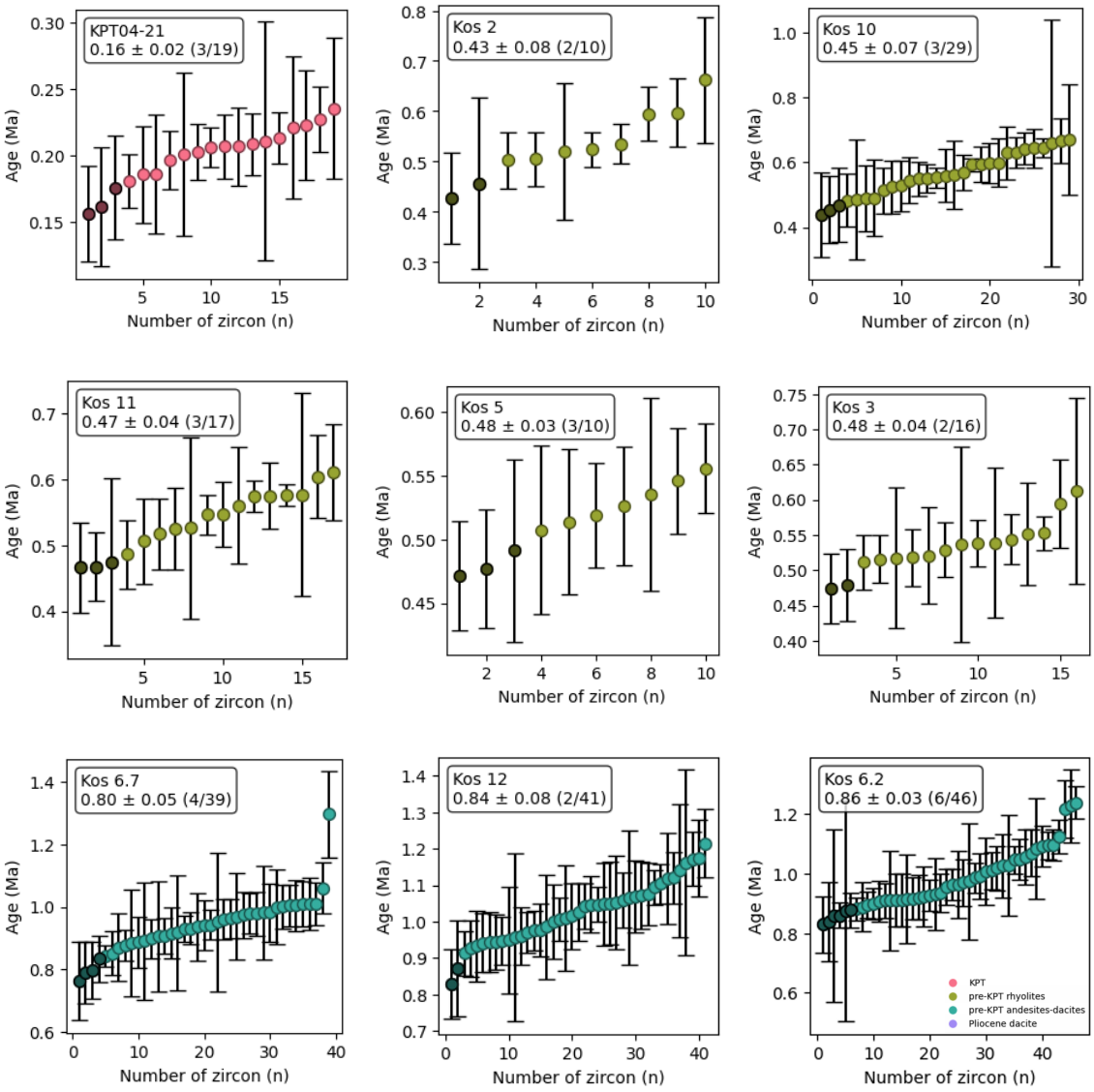

Figure 11 (continued on next page)

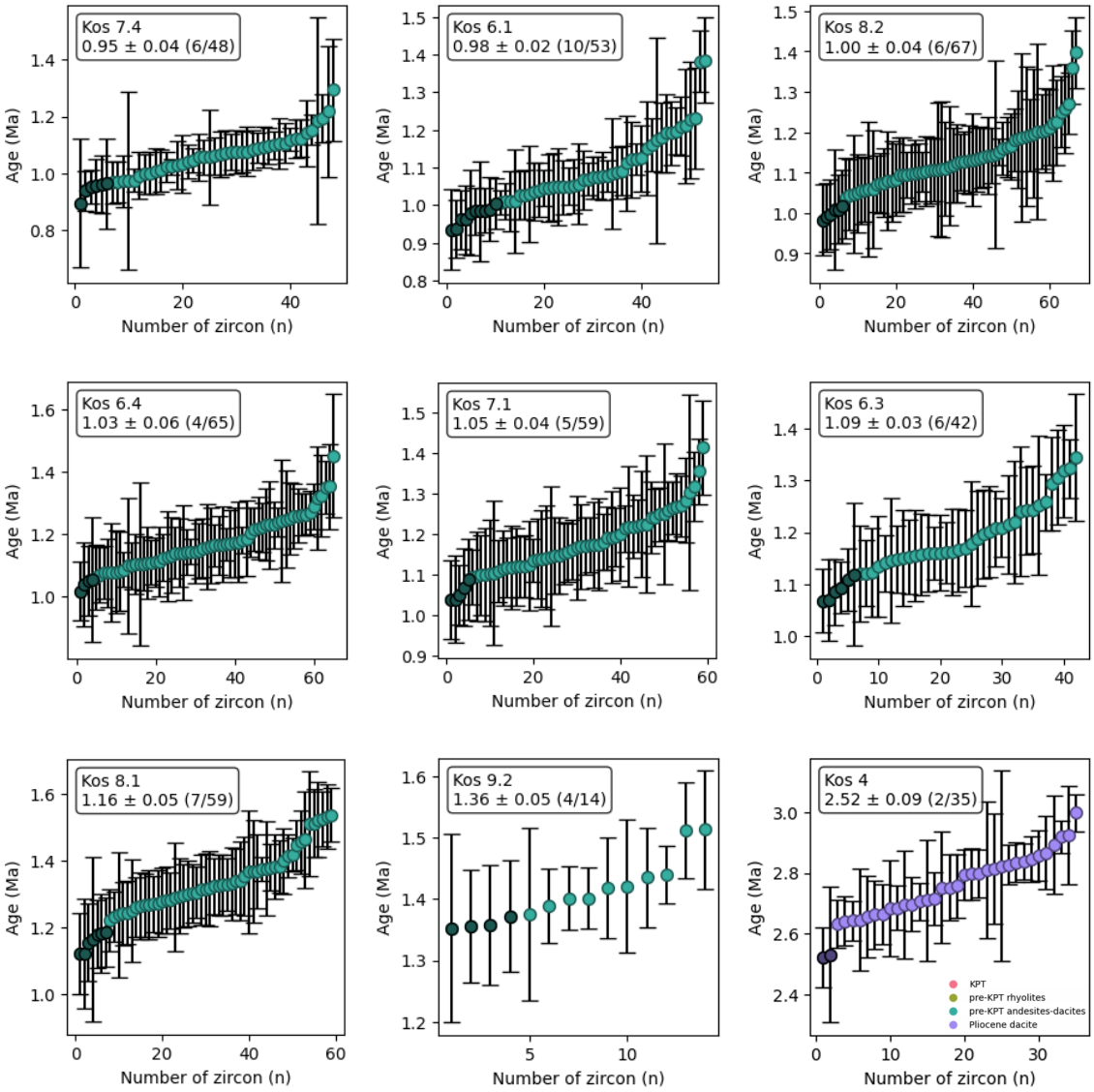

Figure 11: Overview of the zircon crystallization ages for the 18 Kos samples. The uncertainty is shown as 2σ. The crystallization ages were determined using the common Pb correction, which corrected the crystallization ages on the Concordia diagram. The zircons with darker colors represent the youngest zircon populations. In the text box for each sample, the number of crystals in this population is given, along with the total number of zircons that were picked. The color code has been set according to the eruption ages (given in the text box), ranging from the youngest (KPT04-21 (Bachmann et al., 2012; Bachmann, 2010) in red) to the oldest eruption age (Kos 4 in purple).

Table 3: XRF bulk-rock analyses of the main elements (oxides) in the 19 Kos samples. Values are reported in weight percent (wt-%).

	Wt-%										
Sample	SiO_2	Al_2O_3	Fe_2O_3	Na_2O	K_2O	CaO	MgO	MnO	P_2O_5	TiO_2	Total
KPT04-21	70.07	13.19	1.17	4.02	4.22	1.26	0.31	0.05	0.03	0.19	94.51
Kos 1	64.92	16.89	3.72	4.43	2.98	5.09	2.70	0.05	0.15	0.48	101.41
Kos 10	75.63	13.12	0.83	4.66	4.41	0.71	0.11	0.06	*	0.14	99.67
Kos 11	75.58	12.73	0.78	4.48	4.56	0.60	0.12	0.06	*	0.13	99.04
Kos 12	63.37	16.94	4.79	4.58	2.56	5.99	3.20	0.09	0.15	0.61	102.28
Kos 2	75.94	12.98	0.79	4.81	4.19	0.64	0.11	0.06	*	0.13	99.65
Kos 3	75.17	12.76	0.77	4.46	4.40	0.61	0.11	0.06	*	0.12	98.45
Kos 4	65.13	17.38	3.90	4.74	2.86	4.75	2.26	0.04	0.11	0.48	101.65
Kos 5	75.76	12.66	0.76	4.51	4.57	0.70	0.10	0.06	*	0.13	99.24
Kos 6.1	62.20	18.42	4.81	4.47	2.22	7.01	2.73	0.08	0.17	0.67	102.77
Kos 6.2	69.07	16.02	2.59	4.60	3.54	3.94	1.55	0.04	0.12	0.42	101.90
Kos 6.3	62.74	17.50	4.85	4.98	2.43	5.24	2.60	0.08	0.19	0.63	101.24
Kos 6.4	63.08	18.35	3.96	5.08	2.52	6.07	2.12	0.07	0.19	0.68	102.12
Kos 6.7	64.31	16.03	3.56	4.57	2.72	5.04	2.38	0.08	0.13	0.51	99.33
Kos 7.1	63.39	18.86	4.12	5.14	2.56	5.80	1.60	0.05	0.23	0.76	102.51
Kos 7.4	59.86	17.46	4.85	4.64	2.44	5.89	1.52	0.14	0.16	0.65	97.62
Kos 8.1	61.44	18.33	4.83	4.72	2.22	6.58	3.20	0.08	0.20	0.66	102.26
Kos 8.2	63.71	17.92	4.52	4.42	2.78	3.87	1.27	0.05	0.15	0.60	99.30
Kos 9.2	56.56	19.96	5.76	4.91	2.23	8.26	3.72	0.07	0.17	0.66	102.30

* Below LLD

Table 4: XRF bulk-rock analyses of trace elements in the 19 Kos samples are reported in ppm.

	ppm										
Sample	**Rb**	**Ba**	**Sr**	**Zr**	**Y**	**Zn**	**Cu**	**Ni**	**Co**	**Cr**	**V**
KPT04-21	110	999	131	78	*	*	91	40	*	*	*
Kos 1	67	979	790	132	*	75	124	60	*	40	90
Kos 10	114	945	68	82	*	60	88	40	*	*	*
Kos 11	126	997	54	81	*	50	86	30	*	*	*
Kos 12	69	830	492	119	*	79	98	70	20	*	160
Kos 2	117	1000	60	67	14	*	113	40	*	*	*
Kos 3	123	1120	57	73	*	60	139	40	*	*	*
Kos 4	62	950	788	142	*	60	113	70	20	70	*
Kos 5	109	880	55	73	*	50	87	50	*	*	*
Kos 6.1	50	660	525	119	*	79	88	60	*	*	*
Kos 6.2	97	870	433	124	*	70	126	50	*	*	*
Kos 6.3	64	800	590	132	*	81	129	37	*	*	*
Kos 6.4	50	690	664	130	*	75	100	*	10	*	*
Kos 6.7	66	930	503	140	*	76	94	60	*	50	*
Kos 7.1	54	870	664	138	*	60	88	30	*	*	*
Kos 7.4	57	1330	522	123	*	103	104	100	20	*	*
Kos 8.1	50	830	774	122	*	84	106	*	30	*	*
Kos 8.2	76	1040	514	134	*	83	109	40	*	*	*
Kos 9.2	40	467	626	116	*	80	107	90	27	120	*

* Below LLD

Personal Declaration

Personal declaration: I hereby declare that the submitted Thesis is the result of my own, independent work. All external sources are explicitly acknowledged in the Thesis.

April 24, 2025 Céline Mikosch